This is a repository copy of *Numerical and experimental analysis of a multi-directional wind tower integrated with vertically-arranged heat transfer devices (VHTD)*.

White Rose Research Online URL for this paper:
http://eprints.whiterose.ac.uk/104586/

Version: Accepted Version

Article:
Calautit, J.K., Hughes, B.R., O'Connor, D. et al. (1 more author) (2017) Numerical and experimental analysis of a multi-directional wind tower integrated with vertically-arranged heat transfer devices (VHTD). Applied Energy, 185 (2). pp. 1120-1135. ISSN 0306-2619

https://doi.org/10.1016/j.apenergy.2016.02.025

Article available under the terms of the CC-BY-NC-ND licence
(https://creativecommons.org/licenses/by-nc-nd/4.0/)

Reuse
This article is distributed under the terms of the Creative Commons Attribution-NonCommercial-NoDerivs (CC BY-NC-ND) licence. This licence only allows you to download this work and share it with others as long as you credit the authors, but you can't change the article in any way or use it commercially. More information and the full terms of the licence here: https://creativecommons.org/licenses/

Takedown
If you consider content in White Rose Research Online to be in breach of UK law, please notify us by emailing eprints@whiterose.ac.uk including the URL of the record and the reason for the withdrawal request.

eprints@whiterose.ac.uk
https://eprints.whiterose.ac.uk/

Numerical and experimental analysis of a multi-directional wind tower integrated with vertically-arranged heat transfer devices (VHTD)

John Kaiser Calautit – corresponding author (j.calautit@sheffield.ac.uk, Tel: +44(0)7544158981)
Department of Mechanical Engineering, University of Sheffield, Sheffield S10 2TN, UK
Ben Richard Hughes
Department of Mechanical Engineering, University of Sheffield, Sheffield S10 2TN, UK
Dominic O'Connor
Department of Mechanical Engineering, University of Sheffield, Sheffield S10 2TN, UK
Sally Salome Shahzad
Department of Engineering and Technology, University of Derby, Derby, DE22 3AW, UK

Abstract

The aim of this work was to investigate the performance of a multi-directional wind tower integrated with vertically-arranged heat transfer devices (VHTD) using Computational Fluid Dynamics (CFD) and wind tunnel analysis. An experimental scale model was created using 3D printing. The scale model was tested in a uniform flow closed-loop wind tunnel to validate the CFD data. Numerical results of the supply airflow were compared with experimental data. Good agreement was observed between both methods of analysis. The Grid Convergence Method (GCI) method was used to estimate the uncertainty due to discretisation. Results have indicated that the achieved indoor air speed was reduced by 8-17% following the integration of the VHTD. The integration of VHTD had a positive effect on cooling performance of the wind tower, it reduced the incoming fresh air by up to 12K. The effect of varying the number of VHTD rows (1-3rows) on the system's performance were also investigated. Additional simulations were also conducted to investigate the effect of atmospheric boundary layer (ABL) flows on the wind tower ventilation performance and also compare it with the results of uniform flow wind tunnel study.

Keywords: ABL; CFD; hot climates; natural ventilation; wind tunnel

1. Introduction

The building sector has substantial scope to reduce the energy use associated with the operation and maintenance of buildings worldwide. Presently, the building sector contributes

This paper was presented at the 7th International Conference on Applied Energy (ICAE2015), March 28-31, 2015, Abu Dhabi, UAE (Original paper title: **CFD and Wind Tunnel Study of the Performance of a Multi-Directional Wind Tower with Heat Transfer Devices** and Paper No.: **ICAE2015-37**.

30-40% of the global energy demand and more than 60% of this total energy demand is consumed by the Heating, Ventilation and Air-conditioning (HVAC) [1]. This is due to the increasing thermal comfort demands of occupants, regulations for adequate ventilation supply rates and current HVAC technology that is commonly used. Addressing the significant energy requirements of mechanical HVAC services has the potential to significantly reduce the energy demands of buildings heavily reliant on such systems such as commercial buildings, schools and office spaces [2].

Passive ventilation strategies are becoming more commonly used to ventilate and cool buildings [3]. These strategies are able to reduce the energy consumption of buildings with regards to the energy required for ventilation by using the forces of wind driven flow and air buoyancy. Pressure differences created by obstructions in the path of wind flow force air through a building via a combination of driving and suction forces. Air buoyancy due is due to the varying density of air at different temperatures [4]. By controlling this process, buildings can be ventilated with little energy requirement. The two driving forces are combined in a wind tower [5], commercial wind towers have been in existence in the UK for the last 40 years in various forms, and their development over that period has been the subject of much research both in the UK and internationally [6].

Wind towers are passive ventilation systems, based on the traditional vernacular design of baud-geer [7]. Baud-geer have been utilised for centuries, predominantly in Middle East, as a method of delivering ventilation to buildings [7]. Though reducing energy demand through the use of passive ventilation is one solution in cutting greenhouse gases as a result of HVAC systems, the key area for reduction is the conditioning of the air. Unlike air-conditioning, wind towers are ineffective at reducing the temperature of supply air. This places a limit on the application of natural ventilation systems in hot climates [8, 9]. Therefore, additional technologies should be incorporated with the wind tower to cool the airflow. Figure 1a shows a wind tower with evaporative cooling technology. The outdoor airflow entering the wind tower top entrance is passed though evaporative cooling pads, evaporating the water in the process and reducing the airflow temperature. However, there are few issues associated with the method such as high operation and maintenance cost [10]. In addition, evaporative coolers use a substantial amount of water to run. Other drawbacks associated with evaporative cooling are discussed in [10].

In this study, heat transfer devices (HTDs) were incorporated into the internal domain of a multi-directional wind tower to reduce the temperature of supply air. As shown in Figure 1b, the hot outdoor air (1) enters the wind tower through the louvers, which are used to deflect the impact of weather and direct sunshine from entering the device. The airflow is passed through a series of vertically arranged-HTDs (2), which absorbs heat from the airstream and transfers it into a parallel closed-circuit cool sink (3). Volume control dampers are located at the bottom of the unit to control the delivery rate (5). The cooled air is supplied to the room beneath the channel via ceiling diffusers (6). The primary force provides fresh air driven by the positive air pressure on the wind-ward side (1), while exhausting stale air with the assistance of the suction pressure on the leeward side (7).

Figure 1 (a) wind tower with evaporative cooling (b) a multi-directional wind tower with VHTDs.

In our earlier works, we've used numerical modelling to compare the ventilation and thermal performance of a traditional wind tower incorporating evaporative cooling and HTDs [10]. The study showed that the wind tower with HTDs was capable of reducing the air temperature by up to 12-15 K while supplying the recommended fresh air rates. In a more recent work [11], we've explored the integration of horizontally-arranged HTDs into a commercial uni-directional wind catcher. The study identified the cooling potential of the proposed system but also showed several limitations when coupled with a uni-directional system i.e. not suitable in areas with variable wind directions [12]. In this study, we will explore the potential of using a multi-directional device with vertically-arranged HTDs to address this limitation. The system will be capable of supplying fresh air and exhausting stale air irrespective of the wind direction. The numerical model will be validated using a uniform flow wind tunnel. In addition, the effect of varying the number of VHTD rows (1-3rows) on the ventilation and thermal performance will also be investigated. Furthermore, additional simulations were conducted to investigate the effect of ABL flows on the wind tower ventilation performance and also compare it with the uniform flow scenario.

2. Literature Review

The development of several aspects of wind towers to improve efficiency and design has been well documented in the following reviews [13, 14]. A comprehensive review of wind tower development was conducted by Hughes et al. [15]. The most commonly used technique for development are Computational Fluid Dynamics (CFD) modelling and scaled wind tunnel

testing and hence was used in this study. Improvements to traditional wind towers have been investigated in an attempt to increase the effectiveness in providing airflow through the system along with modifications to improve the operation. Bahadori [16] enhanced the cooling potential of wind tower by employing evaporative cooling and used screens at openings to reduce dust infiltration. Using numerical and experimental analysis, Bouchahm et al. [17] made several modifications to a wind tower to improve the effectiveness of the system. The height of the wind tower was increased and partitions within the shaft were introduced to improve the ventilation performance. Wetted surfaces were used to increase the cooling potential through the process of evaporative cooling. Traditional one-sided wind tower models with various types of roofs such as flat, inclined or steep and curved roofs were investigated by Esfeh et al. [18] using wind tunnel testing. Afhsin et al. [19] analysed the natural ventilation performance of a two-sided wind tower for various wind angles and wind speeds by wind tunnel and smoke flow visualisation. Montazeri [20] tested a wind tower design with five different arrangements of cross dividers, this was done to determine the effect of increasing the number of internal sections on the airflow.

Badran [21] investigated the integration of clay conduits inside a wind tower. The results showed that a wind tower with a vertical height of 4metres can decrease the temperature by 11K and generate an airflow of $0.3m^3/s$. The author also concluded that reducing the height of the wind tower which generally reached up to 15metres can decrease the construction cost without having a noticeable decrease in performance. Kalantar [7] evaluated the ventilation and cooling performance of a wind tower in the hot-arid region of Yazd. The work developed a numerical model to analyse the airflow pattern inside the wind tower in three-dimensional and steady-state conditions. The effect of several design parameters such as wind speed, temperature, humidity and density were investigated. Saffari and Hosseinnia [8] also used CFD modelling to investigate the cooling performance of wind towers equipped with wetted curtains under different structural parameters and external conditions. The CFD results showed that the 10m high wetted columns were able to reduce the airflow temperature by 12K and increase the relative humidity of the air by 22%.

Commercial wind towers have been developed through modern, research led interest in optimising the design for maximum airflow rate through the wind tower. The length and number of louvers were optimised by Liu et al. [22] through the use of CFD modelling by evaluating the airflow rate through the wind tower and the uniformity of air distribution

within the wind tower and building. The optimal number of louvers was found to be between 6-8, this was determined by the increase in airflow rate of 12.7% from an initial number of louvers tested as 4 louvers and 5 louvers. The effect of dampers and egg crate grilles on the operation of commercial wind towers was investigated by Elmualim [23]. The work concluded that the addition of dampers and egg crate grilles were capable of reducing airflow through a wind tower by 20-50%. Calautit and Hughes [24] used CFD and wind tunnel testing to investigate the ventilation performance of a four-sided commercial wind tower. The simulation results for indoor airflow rate, supply and extract rates, external airflow and pressure coefficients were compared with measurement results. Jones and Kirby [25] compared the ventilation rate of a variety of ventilation systems by measuring the CO2 concentration in 16 different classrooms. The study found that commercial wind towers were a highly effective method of ventilation during summer months, and effectiveness increased when used in conjunction with open windows.

Recently, the works of Hughes et al. [26] and Calautit et al. [10, 11] proposed that heat transfer devices such as heat pipes could provide the link between passive ventilation and low energy temperature regulation. It had been noted previously that heat pipes integrated into other ventilation systems do not create a significant pressure drop compared to other technology [27], this was critical in the integration into passive ventilation systems as pressure losses should be kept to a minimum. Shao and Riffat [28] were one of the first to explore the use of heat pipes in stack ventilation, however the purpose of the system was to recover the heat from the exhaust stream. The application of heat transfer devices for passive cooling in hot climates was investigated by Calautit et al. [11] by incorporating the technology into a Malqaf uni-directional wind catcher. The study investigated the effect of various outdoor conditions on the performance of the system.

3. Numerical model

The numerical simulations were performed using the commercial CFD code Fluent 14.5. Steady 3D RANS (Reynolds-Averaged Navier-Stokes) CFD simulations were conducted with a standard k-e turbulence model. The rationale behind choosing the k-epsilon model was the findings of previous works on wind towers of the authors [11-12, 29, 31] and also others [13, 16-22, 24] which showed its capabilities in predicting the natural ventilation flows in and around wind towers and also indoor flows [30]. The velocity-pressure coupling was taken care of by the Semi-Implicit Method for Pressure-Linked Equations (SIMPLE) algorithm.

The CFD code used the Finite Volume Method (FVM). Second-order discretisation schemes were used for the convection and viscous terms of the governing equations. The pressure interpolation was second-order. Solution convergence was obtained when the scaled residuals showed no further reduction with increasing number of iterations. The governing equations for the mass conservation (eqn.1), momentum conservation (eqn.2), energy conservation (eqn.3), turbulent kinetic energy (TKE) (eqn.4), energy dissipation rate (eqn.5) and species transport equation are summarised below:

$$\frac{\partial \rho}{\partial t} + \nabla \times (\rho u) = 0 \qquad \text{(eqn.1)}$$

where ρ is density, t is time and u is fluid velocity vector.

$$\frac{\partial(\rho u)}{\partial t} + \nabla \times (\rho u u) = -\nabla \mathrm{p} + \rho \mathrm{g} + \nabla \times (\mu \nabla u) - \nabla \times \tau_t \qquad \text{(eqn.2)}$$

where p is the pressure, g is vector of gravitational acceleration, μ is molecular dynamic viscosity and τ_t is the divergence of the turbulence stresses which accounts for auxiliary stresses due to velocity fluctuations.

$$\frac{\partial(\rho e)}{\partial t} + \nabla \times (\rho e u) = \nabla \times \left(k_{eff} \nabla T\right) - \nabla \times \left(\sum_i h_i j_i\right) \qquad \text{(eqn.3)}$$

where e is the specific internal energy, k_{eff} is the effective heat conductivity, T is the air temperature, h_i is the specific enthalpy of fluid and ji is the mass flux.

$$\frac{\partial(\rho k)}{\partial t} + \nabla \times (\rho k u) = \nabla \times \left[\alpha_k \mu_{eff} \nabla k\right] + G_k + G_b - \rho_\varepsilon \qquad \text{(eqn.4)}$$

$$\frac{\partial(\rho \varepsilon)}{\partial t} + \nabla \times (\rho \varepsilon u) = \nabla \times \left[\alpha_\varepsilon \mu_{eff} \nabla \varepsilon\right] + C_{1\varepsilon} \frac{\varepsilon}{k} (G_k + C_{3\varepsilon} G_b) - C_{2\varepsilon} \rho \frac{\varepsilon^2}{k} \qquad \text{(eqn.5)}$$

where G_k is the source of TKE due to average velocity gradient, G_b is the source of TKE due to buoyancy force, α_k and α_ε are turbulent Prandtls numbers, $C_{1\varepsilon}$, $C_{2\varepsilon}$ and $C_{3\varepsilon}$ are empirical model constants.

$$\frac{\partial}{\partial_t}(\rho Y_i) + \nabla \times (\rho u Y_i) = -\nabla \times \vec{J}_i + R_i + S_i \qquad \text{(eqn.6)}$$

where $\vec{J}_i$ is the diffusion flux of species i, R_i is the net rate of production of species i by reaction and S_i is the rate of creation by addition from the dispersed phase plus any user-defined sources.

3.1 Geometry

Figure 2a shows an exploded view of a standard multi-directional wind tower and a cold sink with vertically-arranged heat transfer devices. The geometry was modelled using a CAD software and the file was exported to ANSYS Workbench, which was used to extract the fluid volumes from the solid CAD model, generate the mesh and perform CFD analysis. The generated computational domain is shown in Figure 3. The computational domain was divided into three volumes: the macro-climate (outdoor environment), wind tower and micro-climate (indoor or test room). It is worth noting that a similar CFD setup was used in previous works on wind tower simulation [11, 31]. The macro-climate volume was modelled around the wind tower to simulate the outdoor airflow. The sizing of the macro-climate volume (5 x 5 x 10m^3) was based on the blockage produced by the object (wind tower) inside the volume. In this case, the wind tower with length, with and height of 1m x 1m x 1.5m produced a blockage of about 5%. It is worth mentioning that this value changes when the wind tower is rotated to simulate different wind directions and as a result, the size of the domain also changes. Airflow was simulated across the macro-climate volume by setting one boundary face as inlet velocity and the opposite face as outlet pressure. In order to assess the performance of the wind tower with VHTD, a micro-climate volume with the dimensions of 3 x 5x 5m^3 was modelled below the system. This micro-climate volume represents a small classroom which can accommodate up to 15 occupants. The system was based on a standard roof-mounted wind tower model [31]. In this study, it was assumed that the system was supplying at 100% (fully-open dampers) hence, the dampers were not included in the model for simplification. It is worth noting that effect of wind tower dampers on ventilation rates was already fully investigated by Elmualim [23]. Figure 2b illustrates the dimension of the HTD and also the spacing between each HTDs. This study will also investigate the effect of varying the number of rows, horizontal spacing and vertical spacing of HTD on the system performance.

Figure 2 (a) CAD model of the wind tower with VHTD (b) VHTD arrangement and spacing (dimension in mm)**.**

3.2 Grid design and verification

Grid generation for complex geometries such as a commercial wind tower model is usually a major tasks hence, a large number of previous works on wind tower modelling [13-15, 23-24] used unstructured grid for discretisation of the computational domain. In order to properly capture the flow fields near the critical areas of interest, such as the louvers and HTD surfaces, size functions were applied to those surfaces. The size of the element was extended to resolve the areas with high-gradient grid and to improve the accuracy of the results of the flow fields [32, 33]. The element size was varied from $5x10^{-3}$ m for the grid near the critical areas to $7x10^{-3}$ m for the middle of the volume. Figure 4 shows the generated grid for the computational domain. The grid had an average wall y+ value of 44.1 over the windward surfaces of the wind tower, 35.1 over the side surfaces and of 20.2 over the leeward surfaces. The maximum y+ value of 120 occurred only at the top and side corners of the wind tower.

Figure 3 Grid generation on the computational domain.

In order to verify the accuracy of the numerical model, a grid sensitivity analysis was conducted to determine the variation in results over different grid sizes. It is worth noting that before conducting the discretisation error estimation, it was ensured that iterative convergence was achieved (as detailed in Section 3.4). In this study, the Grid Convergence Method (GCI) method (based on the Richardson extrapolation method) was selected to estimate the uncertainty due to discretisation [34-36]. The procedure detailed in [35] was followed and is summarised below:

The first step is to define a representative grid size h.

$$h = \left[\frac{1}{C}\sum_{i=1}^{C}(\Delta V_i)\right]^{1/3} \quad \text{(eqn.7)}$$

where C is the total number of cells used for the 3D computations and ΔV_i is the volume.

The next step is to select three significantly different set of grids, C and run simulations to determine the values of key variables, $\emptyset$. In this case, the velocity at different height inside the room model was selected as the variable. According to [35], it is desirable that refinement factor $r = h_{coarse}/h_{fin}e$ to be greater than 1.3. Therefore, the size of the grids were C1 (12,932,488), C2 (6,847,693) and C3 (4,046,918), giving r values of 1.37 and 1.30.

The next step is to calculate the apparent order, p of the method using the next equation. The equation was solved using fixed point iteration, with the initial guess equal to the first term [35].

$$p = \frac{1}{\ln(r_{21})} |ln|\varepsilon_{32}/\varepsilon_{21}| + q(p)| \quad \text{(eqn.8)}$$

$$q(p) = ln\left(\frac{r_{21}^{p} - [1 \times sgn(\varepsilon_{32}/\varepsilon_{21})]}{32 - [1 \times sgn(\varepsilon_{32}/\varepsilon_{21})]}\right) \quad \text{(eqn.9)}$$

where $\varepsilon_{32} = \emptyset_3 - \emptyset_2$ and $\varepsilon_{21} = \emptyset_2 - \emptyset_1$.

Finally, the approximate relative error e_a^{21}, extrapolated relative error $\emptyset_{ext}^{21}$ and fine-grid convergence index GCI_{fine}^{21}(eqn.11) are calculated. Table 1 shows examples of the calculation procedure for the three selected grids. According to Table 1, the numerical uncertainty in the fine-grid solution for the velocity at 1.67 was 5.25% which corresponded to ± 0.077 m/s.

Table 1 Sample calculations of discretisation error using the GCI method.

Figure 4a shows the vertical velocity profiles (line with 14 equally distributed points) drawn from the supply quadrant of the wind tower to the bottom of the floor, which was based on the three set grids. In addition, the extrapolated values, $\emptyset_{ext}^{21}$ are also plotted and was calculated using the following equation:

$$\emptyset_{ext}^{21} = \left(r_{21}^{p}\emptyset_1 - \emptyset_2\right)/\left(r_{21}^{p} - 1\right) \quad \text{(eqn.10)}$$

The local order of accuracy p ranged from 1.4 to 5.7. The average apparent order of accuracy was used to assess the GCI index values in eqn.11, which is plotted in the form of error bars, as shown in Figure 4b. Based on the fine-grid convergence index, the maximum discretization uncertainty was 6.61% which corresponded to ± 0.087 m/s. The discretisation uncertainty value ranged from 0.31% to 6.61%, with a global average of 2.63%.

$$GCI_{fine}^{21} = \frac{1.25e_a^{21}}{r_{21}^{p} - 1} \quad \text{(eqn.11)}$$

Figure 4 Grid verification using the Grid Convergence (GCI) method. (a) plot of the velocity profiles drawn from a line extending from the supply to the floor; (b) fine grid solution, with discretization error bars computed using the GCI index.

3.3 Cell zone and boundary conditions

The cell zone and boundary conditions for the numerical model are summarised in Figure 5. In order to investigate the impact of varying wind speed, the velocity inlet was varied between 1– 5m/s. In order to replicate the wind tunnel flow conditions, a uniform velocity inlet profile was simulated. It is worth noting that several previous works [13-20] have also used this method for setting the inflow conditions. The measured turbulence intensity [38] was also used as inlet boundary condition. The pressure outlet was set to 0Pa (zero static pressure). The outdoor air temperature was set to 318 K to simulate a hot outdoor environment. The surface of the HTD was set to wall with constant surface temperature [10, 26]. All the volumes were set to fluid zones and the material was set to air (default material properties in Fluent).

Figure 5 Set boundary conditions for the computational domain's volumes and surfaces.

3.4 Criteria for solution convergence

Solution convergence is the term for a numerical method using iterations to produce a solution of the numerical grid, whereby the error approaches zero. Solutions are based on iterations against pre-defined convergence criterion [33]. The default values for the convergence criterion is 10^{-6} for the energy equation and 10^{-3} for all other equations. The iteration process is complete when the set convergence criterions are met. However, according to Fluent guidelines [33], this criterion may not be appropriate for all types of simulations and it is a good idea to judge convergence by monitoring the residuals. In this study, the convergence criterion was set to none and the convergence was monitored by examining the residuals chart as shown in Figure 6. Relevant integrated quantities such as the supply and indoor velocity (Figure 7a, 7b) and temperature (Figure 7c, 7d) were also monitored. Convergence was achieved when the average airflow speed and temperature at this locations were stable for around 500 iterations. In addition to monitoring residuals and solution variables, the property conservation was also checked if satisfied [33]. This was carried out by performing a mass flux balance and heat transfer rate balance for the converged solution. This option was available in the FLUENT flux report panel which allows computation of mass flow rate and total heat transfer rate for the selected boundary zones.

For the simulation of wind tower in 3m/s wind, the mass flow rate balance was 1.82e-05kg/s which was below the required value or <1% of smallest flux through domain boundary [33].

Figure 6 Residuals chart within the Fluent solver.

Figure 7 Convergence monitoring of (a) supply velocity (b) indoor velocity (c) supply temperature and (d) indoor temperature.

3.5 Atmospheric boundary layer (ABL) flow simulation of the VHTD wind tower

In order to investigate the ventilation performance of the system in atmospheric boundary layer (ABL) flows, additional simulations were conducted. Due to the limitation of the wind tunnel and to simplify the model, the flow profile that was used in the initial simulations (as described in the Section 3.3) was based on the wind flow simulated by the wind tunnel which was nearly uniform. However, this does not take into account the frictional drag of the ground surface which generates a boundary layer in which there is a progressive reduction in wind speed towards the ground as described by [39]. Hence, the study will carry out additional simulations to investigate its effect on the wind tower performance.

For this simulation, the domain was adequately large to prevent artificial acceleration of the flow as shown in Figure 8. The inlet, the lateral and the top boundary was 5H away from the building or room, where H is the room height. The outlet boundary was positioned 15H behind the building, sufficiently long to allow the wake region development behind room [40]. Similarly, the domain consisted of an inlet on one side and an outlet on the opposing boundary wall. Similar grid method was used for this study. The boundary conditions were set using the guidelines highlighted by [39] for the simulation of flows in the urban environment. The vertical profiles of the airflow velocity U and TKE k were imposed on the inlet as shown in Figure 9, based on the measurement data of [39]. The mean speed of the approach flow (Figure 9a) obeyed a power-law with α = 0.25, which corresponds to a sub-urban terrain. Uref is the value of the velocity at a height of 3.6m which is the height of the inlet opening of the wind tower. This value was varied between 1-5 m/s and the CFD results of the supply velocity were directly compared to the results of the uniform flow simulations which were also run between 1-5 m/s. This ensured that the velocity of the wind flow at wind tower opening height were similar and would be better method for comparing the uniform

flow and ABL flow simulations. For the k-ε model, the values of ε were obtained by assuming local equilibrium of $Pk = \varepsilon$. From Figure 8, the top and side boundaries were defined as symmetry and similarly the outlet of the domain was set to 0Pa. All the test room surfaces were set as smooth non-slip walls. The standard wall functions were prescribed to the wall boundaries [41]. The wall functions for the ground surface were modified as proposed by [42] to reflect the effect of roughness of the ground using the equivalent sand-grain roughness height ks and roughness constant Cs.

Figure 8 Computational domain for the analysis of the VHTD wind tower in ABL flows.

Figure 9 Vertical profiles of (a) mean velocity U and (b) turbulent kinetic energy k in the approaching ABL flow [39].

4. Experimental wind tunnel tests

Experimental testing was conducted using a low-speed closed-loop wind tunnel displayed in Figure 10. The wind tunnel had a test section with cross-sectional area of 0.5x0.5m^2 and length of 1m. It is worth noting that the test section is a scaled-down version (1:10) of the macro-climate of the numerical model. The specifications and characterisation of the wind tunnel are fully detailed in [37]. Similar to the numerical model, the wind tower was positioned at the centre of the test section and a test room was located beneath it. At 1:10 scale the model generates a blockage of about 5%, this value was acceptable and no corrections were required to be made to the airflow measurements [18-20, 37]. To have wind tunnel experiment outcomes which can be transferred to full scale, the model in the wind tunnel and outdoor must have geometric and dynamic similarity [43, 44]. The geometric similarity between the numerical model and wind tunnel prototype was maintained by equally scaling down the dimensions of the prototype by 1:10. In order to achieve dynamic similarity, the Reynolds number of the model must also equal that of the actual. In this case if the actual building was in a wind flow of 1m/s, to have the same Reynolds number in the test section with an object scale of 1:10, the velocity should be 10 times as larger or 10m/s. The wind tunnel speed was set to 10m/s to achieve this requirement.

Figure 10 Front view of the closed-loop low-speed wind tunnel [37].

4.1 Scale wind tower model

All of the parts of the wind tower scale model were created using 3D printing, except for the HTDs which were modelled using cylindrical copper rods with $2x10^{-3}$m diameter. The top section of the wind tower which was the cold sink was modelled as as a solid block with the HTD hole patterns so that the cylindrical rods can be slotted in and ensure accurate positioning of the HTD. It is worth noting that only the air velocity was investigated during the experimental tests because the thermal properties of a full-size HTD could not be replicated at 1:10 scale. Underneath the wind tower was a test room with a floor area of $0.5x0.5m^2$ and vertical height of 0.3m. The test room was constructed using a transparent material to facilitate smoke visualisation. Figure 11 shows an exploded view of the 3D printed model of the wind tower with VHTD.

Figure 11 A 1:10 3D-printed model of the VHTD wind tower for the wind tunnel tests.

4.2 Measurement techniques

4.2.1 Volumetric flow supply rate

The velocity of the airflow beneath the channel of the wind tower was measured using a hot-wire anemometer, due to its fast response times and capability of measuring low air velocities, which were present during this investigation. The cross-sectional area of the wind tower channel was divided into several portions and the airflow rate through it was calculated as follows:

$$Q = \sum_{i=1}^{n} A_i \times U_i \qquad \text{(eqn.12)}$$

Where Q is the airflow rate through the wind tower channel, A_i is the area of point i and U_i is the velocity of point i. Figure 12a displays the position of the points inside the wind tower channel. The hot-wire anemometer used was a Testo 425, which gave velocity measurements with uncertainty of $\pm$1.0% of rdg. at speeds below 8m/s (Figure 12b). The instrument covers the air velocity range from 0 to 20 m/s and the temperature range from -20 to 70°C. Measurement for each point was taken and averaged over a two minutes period.

Figure 12 (a) Section view of the wind tower supply channel showing the location of the measurement points (dimensions in mm) (b) hot-wire anemometer.

4.2.2 Airflow visualisation

In order to recognise the flow pattern inside the test room, smoke visualisation test was conducted. Figure 13 shows the smoke visualisation setup in the wind tunnel. The AFA-10 unit was used for the smoke generation. The unit is mainly used in subsonic wind tunnels and other low flow rate air flow applications. It has control unit that pumps smoke oil to the tip of a probe. A low-voltage electrical coil at the probe tip heats the oil to produce a fine smoke trail. The model was exposed to a free stream air velocity of 3 m/s to reach a high concentration of the smoke that was sufficient for visualisation. In addition, a high speed camera (EoSens Cube7**)** was used to record and analyse the movement of smoke-visualised airflow paths inside the room.

Figure 13 Experimental airflow visualisation test setup.

5. Validation of the numerical method

5.1 Supply and exhaust airflow measurements

Figure 14 compares the predicted and measured results of the airflow velocity below the wind tower channel. The maximum airflow speed was measured near the center of the wind tower's cross-divider at the supply side (Point 3), this was consistent with the numerical results. The lowest airflow speed was observed in the leeward-exhaust quadrant. Overall, the trend showed that the numerical model was capable of predicting the airflow velocity in the supply and exhaust channels. Average error across the points was 4.53%. To compare the average error by quadrant, the supply quadrant (Points 1-5) had an average error of 2.10% while the exhaust quadrants (Points 6-20) had an average error of 5.34%. The error for all the points were all below 10.00% except for Point 18, which had an error of 19.65% corresponding to ± 0.039 m/s.

Figure 14 Comparison between predicted and measurement results of the airflow velocity.

5.2 Indoor airflow pattern

Figure 15 compares the predicted and visualised airflow pattern inside the test room. A very similar pattern was observed between both methods. As the airflow enters the space through the wind tower, it was directed towards the floor (Figure 15c) of the ventilated space and spread outwards in all directions. The airflow slows down as it moves across the floor and then to the side walls, which created large recirculation regions from all corners (Figure 15d).

An increased amount of smoke was observed at the leeward side of the wind tower when the entire volume of the room was filled with smoke (Figure 15e), which was due to the exhaust quadrants pulling the air out of the space. The results confirmed that the addition of the vertically-arranged heat transfer devices did not impede the airflow from flowing in and out of the wind tower. It can also be argued that its impact on the performance of the wind tower was minimal when comparing the smoke tests of a wind tower with and without HTD (last image). Since the focus of this study was to investigate the indoor airflow, the smoke generator tip was placed closer to the inlet of the wind tower and the high speed camera was setup to capture this pattern. Although, some of the airflow which flows around the wind tower, particularly on top, can be clearly seen in the images.

Figure 15 (a) CFD predicted streamlines and video stills of smoke visualisation at (b) 320 millisecond (c) 1000 millisecond (d) 1700 millisecond (e) 3500 millisecond. For comparison, last image shows smoke test of a standard wind tower at 1000 millisecond.

6. Results and Discussion

5.1 Velocity distribution: standard vs. VHTD wind tower

Figure 16a displays the velocity contours of a cross-sectional plane in the computational domain of the standard wind tower model. The colour map on the left represents the magnitude of the air velocity. From the diagram, the airflow in the macro-climate entered from the right inlet wall at 3m/s and decelerated up to 1m/s as it approached the windward side of the wind tower. Then, the airflow split with some entered the opening through the angled louvers and some passed around the sides and top of the wind tower and traveled towards the pressure outlet wall. A recirculation region was formed on the leeward side of the wind tower which extracted the air from the micro-climate through the leeward openings. The flow entering the wind tower was accelerated up to 3m/s and re-directed down into the space. Since there were no volume control dampers in the model, high velocity drafts were observed at the middle of the space reaching up to 1.8m/s. The average speed inside the volume was 0.22m/s. Figure 16b displays the effect of the addition of the VHTDs on the indoor airflow distribution. From the contour plots, it can be observed that a very similar airflow pattern was predicted by the CFD model which indicated that the VHTDs had little effect on the airflow. The average velocity at the supply was 1.65m/s, which was 0.18 m/s lower than what was achieved by a standard wind tower.

Figure 16 Velocity contour plot of a cross-sectional plane: (**a**) standard wind tower and (**b**) wind tower with vertically-arranged heat transfer devices.

5.2 Pressure distribution: standard vs. VHTD wind tower

Figure 17a displays the total pressure contours of a cross-sectional plane in the computational domain of a standard wind tower model. The average total pressure inside the ventilated space was -1.23 Pa (measured from 5 equally distributed horizontal planes), a negative pressure value, which indicated that the exhaust rates were higher than the supply rates. In this case, 3 openings were used for extraction of stale air and only 1 for supplying fresh air. The addition of VHTDs reduced the average total pressure inside the space to -1.51Pa indicating that the supply rate was slightly reduced. The zoomed in images of the supply channel of the wind tower further demonstrated the reduction in pressure due to the VHTDs.

Figure 17 Total pressure contour plot of a cross-sectional plane: (**a**) standard wind tower and (**b**) wind tower with vertically-arranged heat transfer devices.

5.3 Ventilation rates: standard vs. VHTD wind tower

The numerical models were run for different inlet wind speeds (1 – 5 m/s) to calculate the supply rates in L/s (Figure 18a) and L/s per occupant (Figure 18b). The addition of HTDs reduced the supply rates of the wind tower by 8-17%. According to the CIBSE ventilation guidelines [45], the minimum required supply rate for classroom spaces is 8 L/s per person and 10L/s is the recommended rate for office spaces.

Figure 18 Comparison between the (**a**) airflow supply rates (**b**) L/s per occupant of a standard and VHTD wind tower. Blue dotted lines indicate recommended rate for offices and red dotted lines minimum requirement for classrooms.

5.4 Temperature and humidity distribution

Figure 19a displays the temperature contours of a cross-sectional plane in the computational domain of a wind tower with VHTD. The left hand side of the contour plot shows the scale of static temperature (K). The average temperature inside the room was 310.2 when the otdoor air temperature was set at 318K and wind speed to 3m/s. The predicted results showed reduction in the air temperature was observed after the heat transfer devices. Furthermore, the temperature of the airflow in the right area of the ventilated space was at a lower temperature as compared to the left area. This was due to the direction of the cooler inlet air temperature

moving into the room along with the effect of pressure on the leeward side of the wind tower, extracting air from the space. Figure 19b displays the result of increasing the outdoor wind speeds (1 – 5 m/s) on the thermal performance. As expected, the cooling performance of the HTD reduced as the airflow velocity increased. For example, at 5m/s wind velocity, the temperature was reduced by 5.6K. While at 2m/s, temperature reduction of up to 9.2K was observed.

Figure 19 (**a**) Static temperature contour plot of a cross-sectional plane wind tower with vertically-arranged heat transfer devices (**b**) Effect of various outdoor wind speed on average supply temperature.

Figure 20 displays the simulated result of increasing the outdoor relative humdity (20% - 50%) on the supply and indoor humidity levels. As observed, the airflow relative humdity was increased by 33.5-36.8% (34.7% on average) as a result of temperature reduction.

Figure 20 Effect of outdoor relative humidity on average supply temperature, with the outdoor velocity and temperature set at 3m/s and 318K.

5.5 Heat transfer device (HTD) arrangement

5.5.1 Effect of the variation of the number of HTD rows on performance

Figure 21 and 22 shows the effect of increasing the number of HTD (from 1 row to 3 rows) on the thermal and ventilation performance of the system. It was observed that increasing the number of rows from 1 to 2 rows improved the thermal performance by 33.6-77.2% and increasing from 2 to 3 rows improved the thermal performance by 28-47.5%. Clearly, using more HTDs or rows of HTDs improved the cooling performance of the system while its effect on the ventilation rates was lower as observed in Figure 19.

Figure 21 Effect of the variation of HTD rows on supply temperature reduction.

Figure 22 Effect of the variation of HTD rows on (**a**) supply and (**b**) exhaust velocity.

5.6 Impact of ABL flow on ventilation performance

Figure 23 illustrates the contours of velocity and airflow streamlines in the vertical plane drawn from the middle of the domain which is aligned with the direction of the flow and

contains the centre of the wind tower. The approach ABL flow entering from right causes high pressure on the façade it is hitting and as the wind goes around the corner of the building it cavitates and speeds up considerably, generating strong negative pressure at the corners and less strong negative pressure on the rest of the building walls. It can also be observed that the flow path rises over the building (lift) and accelerates, creating flow separation by the building edge. In the uniform flow model (See Figure 16), the test room or building in the outdoor domain was not included hence this effect was not captured and would likely reduce the performance of the wind tower. Some of the air entered the wind tower via the angled louvers and some passed on top or moved around the sides and exited the pressure-outlet boundary. After passing the louvers, the airflow that entered the wind tower was deflected upwards. The flow was observed to be slightly accelerated as it turns sharply inside the 90° corner. As expected, reduction in speed was observed downstream of the heat transfer devices. A column of fast moving air enters the room, where the airstream hit the floor of the room and moves toward the opening on the right wall. The airflow distribution inside the building was similar to the uniform flow model (See Figure 16). The main difference was the velocity of the flow inside and below the wind tower, which was reduced as it can be seen in Figure 23. It is worth mentioning that for both models, the airflow velocity at the height of the opening of wind tower (3.6m) was about 3m/s. A large recirculation zone with comparatively low airflow velocities was observed at the back of the test room and wind tower.

Figure 24 compares the average the average airflow supply speed of the wind tower with heat transfer devices in uniform and atmospheric boundary layer (ABL) flows. It was observed that the results follow a similar trend for both cases, with the wind tower in uniform flow supplying 20.45-22.92% higher than the one in ABL flow which obeyed power-law with α = 0.25 (sub-urban). As discussed previously, in order to have a fair comparison between the uniform flow and ABL flow simulations, the uniform flow velocity was varied between 1-5 m/s and the value of Uref (velocity at wind tower opening height) of the ABL flow profile were also varied between 1-5 m/s. This ensured that the velocity of the wind flow at wind tower opening height were similar.

Figure 23 Distribution of the predicted velocity magnitude (m/s) for a wind tower with vertically-arranged heat transfer devices in ABL flows.

Figure 24 Comparison between the supply speed of the wind tower in uniform and ABL flows ($\alpha = 0.25$) at various outdoor speeds.

7. Conclusion and Future Work

The recent innovation of commercial wind towers is an example of bringing traditional solutions up to date with contemporary practices. Using modern engineering and design techniques applied to the design principles of the baud-geer, commercial wind towers are able to fill the gap of low energy ventilation solutions. The goal of this study was to explore the potential of incorporating vertically-arranged heat transfer (VHTD) device into a multi-directional wind tower system in terms of reducing the temperature of the airflow and also maintaining the fresh air rates. This study introduced and discussed the potential of this concept through the use of numerical modelling and uniform flow wind tunnel experiments for validation of the method. The experimental model was created using 3D printing and tested in a low-speed wind tunnel. To have wind tunnel experiment outcomes which can be transferred to full scale, the model in the wind tunnel and outdoor achieve geometric and dynamic similarity. The numerical results for the air supply rates were validated against the experimental data and good agreement between both methods was observed. The average error between predicted and measurements across the points was 4.53% and even lower error was observed in the measurements in supply channel which was 2.10%. Smoke visualisation experiment was conducted to further investigate the indoor airflow patter. The results of this experiment confirmed that the addition of the VHTDs did not impede the supply and exhaust airflow. The accuracy of the numerical modelling was also verified by performing grid sensitivity analysis by determine the variation in results over different grid sizes. The Grid Convergence Method (GCI) method was selected to estimate the uncertainty due to discretization. Based on the fine-grid convergence index, the maximum discretisation uncertainty was 6.61% which corresponded to ± 0.087 m/s. The discretisation uncertainty value ranged from 0.31% to 6.61%, with a global average of 2.63%.

The numerical analysis was conducted to simulate and investigate the airflow and temperature distribution inside the wind tower and the test room model. A standard wind tower was utilised as a simulation benchmark model for comparison of the ventilation performance. Findings of the airflow analysis indicated that the supply rate was slightly reduced following the integration of the VHTD, reductions of 8–17% were calculated from the numerical model. This results were consistent with the data of the wind tunnel tests and

the pressure distribution analysis. In addition, the results also showed that proposed system was capable of supplying the required fresh air rates (10L/s per person) even at low wind speeds (2-5m/s). The addition of VHTDs had a positive effect on thermal performance of the wind tower, it reduced the incoming fresh air (318 K) by up to 12 K. Simulation of various outdoor wind velocities (1-5m/s) showed that the cooling performance of the HTDs was indirectly proportional with the ventilation rate. For example, at 5m/s wind velocity, the temperature was reduced by 5.6K. While at 2m/s, temperature reductions of up to 9.2 was observed. The number of HTD rows was varied to optimise the cooling and natural ventilation performance.

Furthermore, additional simulations were also conducted to investigate the effect of atmospheric boundary layer (ABL) flows on the wind tower ventilation performance and also compare it with the results of uniform flow wind tunnel study. Overall, a similar indoor flow distribution was observed in both cases but the velocity of the airflow supplied by the wind tower in uniform flows was slightly higher. The results of various wind speed simulations showed that the wind tower in uniform flow supplied 20.45-22.92% higher than the wind tower in ABL flow. There are two main reasons for this difference; the inclusion of the building geometry in the outdoor domain and the use of a sub-urban approach flow.

This study demonstrated the positive effect of the integration of HTD on the thermal performance of a multi-directional wind tower but also revealed technical issues which remain to be solved such as control strategy and cold sink operation. Another method which could further improve the thermal performance is the addition of extended surfaces. Full-scale testing of the system is required to characterise its performance under real operating conditions and also to further validate the results of this study particularly the cooling performance. Finally, laboratory testing of the model in a wind tunnel capable of simulating ABL flows is recommended.

Acknowledgement

The support by the University of Sheffield (Department of Mechanical Engineering) is gratefully acknowledged. The statements made herein are solely the responsibility of the authors.

Reference

[1] Rahman MM, Rasul MG, Khan MMK, Energy conservation measures in an institutional building in sub-tropical climate in Australia, **Applied Energy**, 2010, 87, 2994-3004.

[2] Yau YH, Lee SK, Feasibility study of an ice slurry-cooling coil for HVAC and R systems in a tropical building, **Applied Energy**, 2010, 87, 2699-2711.

[3] Sofotasiou P, Hughes BR, Calautit JK, Qatar 2022: Facing the FIFA World Cup climatic and legacy challenges, **Sustainable Cities and Society**,2015, 14, 16-30.

[4] Woods AW, Fitzgerald S, Livermore S, A comparison of winter pre-heating requirements for natural displacement and natural mixing ventilation, **Energy and Buildings,** 2009, 41, 1306-1312.

[5] Calautit JK, Hughes BR, Ghani SA, A Numerical Investigation into the Feasibility of Integrating Green Building Technologies into Row Houses in the Middle East, **Architectural Science Review**, 2013, 56, 279-296.

[6] O'Connor D, Calautit JK, Hughes BR, A Study of Passive Ventilation Integrated with Heat Recovery, **Energy and Buildings**, 2014, 82, 799-811.

[7] Kalantar V, Numerical simulation of cooling performance of wind tower (Baud-Geer) in hot and arid region, **Renewable Energy**, 2009, 34, 246-254.

[8] Saffari H, Hosseinnia SM, Two-phase Euler-Lagrange CFD simulation of evaporative cooling in a Wind Tower, **Energy and Buildings**, 2009, 41, 991-1000.

[9] Abro R, Recognition of passive cooling techniques, **Renewable Energy**, 1994, 5, 1143-1146.

[10] Calautit JK, Chaudhry HN, Hughes BR, Ghani SA, Comparison between evaporative cooling and heat pipe assisted thermal loop for a commercial wind tower in hot and dry climatic conditions, **Applied Energy**, 2013, 101, 740-755.

[11] Calautit JK, Hughes BR, Shahzad SS, CFD and wind tunnel study of the performance of a uni-directional wind catcher with heat transfer devices, **Renewable Energy**, 2015, 83, 85-99.

[12] Calautit JK, O'Connor D, Sofotasiou P, Hughes BR, CFD Simulation and Optimisation of a Low Energy Ventilation and Cooling System, **Computation**, 2015, 3, 128-149.

[13] Saadatian O, Haw LC, Sopian K, Sulaiman MY, Review of windcatcher technologies, **Renewable and Sustainable Energy Reviews**, 2012, 16, 1477-1495.

[14] O'Connor D, Calautit JK, Hughes BR, A review of heat recovery technology for passive ventilation applications, **Renewable and Sustainable Energy Reviews**, 2016, 54, 1481-1493.

[15] Hughes BR, Calautit JK, Ghani SA, The Development of Commercial Wind Towers for Natural Ventilation: a review, **Applied Energy**, 2012, 92, 606-627.

[16] Bahadori M, Mazidi M, Dehghani AR, Experimental investigation of new designs of wind towers, **Renewable Energy**, 2008, 33, 2273–2281.

[17] Bouchahm Y, Bourbia F, Belhamri A, Performance analysis and improvement of the use of wind tower in hot dry climate, **Renewable Energy**, 2011, 36, 898-906.

[18] Esfeh MK, Dehghan AA, Manshadi MD, Mohagheghian S, Visualized flow structure around and inside of one-sided wind-catchers, **Energy and Buildings**, 2012, 55, 545-552.

[19] Afshin M, Sohankar A, Manshadi MD, Esfeh MK, An experimental study on the evaluation of natural ventilation performance of a two-sided wind-catcher for various wind angles, **Renewable Energy**, 2016, 85, 1068-1078.

[20] Montazeri H, Experimental and numerical study on natural ventilation performance of various multi-opening wind catchers, **Building and Environment**, 2011, 46, 370-378.

[21] Badran AA, Performance of cool towers under various climates in Jordan, **Energy and Buildings**, 2003, 35, 1031-1035.

[22] Liu SC, Mak CM, Niu JL, Numerical Evaluation of Louver Configuration and Ventilation Strategies for the Windcatcher System, **Building and Environment**, 2011, 46, 1600-1616.
[23] Elmualim A, Effect of damper and heat source on wind catcher natural ventilation performance, **Energy and Buildings**, 2006, 38, 939–948.
[24] Calautit JK, Hughes BR, Wind tunnel and CFD study of the natural ventilation performance of a commercial multi-directional wind tower, **Building and Environment**, 2014, 80, 71-83.
[25] Jones BM, Kirby R, The performance of natural ventilation windcatchers in schools - A comparison between prediction and measurement, **International Journal of Ventilation**, 2010, 9, 273-286.
[26] Hughes BR, Chaudhry HN, Calautit JK, Passive energy recovery from natural ventilation air streams, **Applied Energy**, 2014, 113, 127-140.
[27] Shao L, Riffat SB, Flow loss caused by heat pipes in natural ventilation stacks, **Applied Thermal Engineering**, 1997, 17, 393-399
[28] Riffat SB, and Gan G, Determination of effectiveness of heat-pipe heat recovery for naturally-ventilated buildings, **Applied Thermal Engineering**, 1998, 18, 121-130.
[29] Calautit JK, O'Connor D, Hughes BR, Determining the optimum spacing and arrangement for commercial wind towers for ventilation performance, **Building and Environment**, 2014, 82, 274-287.
[30] Sofotasiou P, Calautit JK, Hughes BR, O'Connor D, Towards an integrated computational method to determine internal spaces for optimum environmental conditions, **Computer and Fluids**, 2016, 127, 146-160.
[31] Calautit JK, Hughes BR, Measurement and prediction of the indoor airflow in a room ventilated with a commercial wind tower, **Energy and Buildings**, 2014, 84, 367-377.
[32] Chung T, Computational fluid dynamics, Cambridge University Press, 2002, 1, 15-21.
[33] ANSYS® Academic Research. ANSYS FLUENT User's Guide Release 14.0. Pennsylvania: ANSYS, Inc; 2014.
[34] Roache PJ, Conservatism of the GCI in Finite Volume Computations on Steady State Fluid Flow and Heat Transfer, 2003, **ASME J. Fluids Eng.**, 125,731–732.
[35] Celik I, Ghia U, Roache PJ, Freitas CJ, Coleman H, Raad PE, Procedure for Estimation and Reporting of Uncertainty Due to Discretization in CFD Applications. **ASME. J. Fluids Eng.**, 2008, 130.
[36] Roache PJ, A Method for Uniform Reporting of Grid Refinement Studies, 1993, **Proceedings of Quantification of Uncertainty in Computation Fluid Dynamics,** ASME Fluids Engineering Division Spring Meeting, Washington, D.C., June 23–24.
[37] Calautit JK, Hughes BR, Integration and application of passive cooling within a wind tower for hot climates, **HVAC&R Research**, 2014, 20, 722-730.
[38] Calautit JK, Chaudhry HN, Hughes BR, Sim LF, A validated design methodology for a closed-loop subsonic wind tunnel**, Journal of Wind Engineering and Industrial Aerodynamics**, 2014, 125, 180-194.
[39] Tominaga Y, Akabayashi S, Kitahara T, Arinami Y, Air flow around isolated gable-roof buildings with different roof pitches: Wind tunnel experiments and CFD simulations, **Building and Environment**, 2015, 84, 204-213.
[40] Franke J, Hirsch C, Jensen AG, Krüs HW, Schatzmann M, Westbury PS, Miles SD, Wisse JA, Wright NG, Recommendations on the use of CFD in wind engineering, 2004, **In Cost action C**, 14, C1.
[41] Launder BE, Spalding DB, The numerical computation of turbulent flows, **Computer Methods in Applied Mechanics and Engineering**, 1974, 3, 269–289.

[42] Blocken B, Stathopoulos T, Carmeliet J, CFD simulation of the atmospheric boundary layer: wall function problems, **Atmos Environ**, 2007, 41, 238–252.
[43] Cermak J, Isyumov N, Wind tunnel studies of buildings and structure, **ASCE Publications**, 1999.
[44] Jensen M, The model-law for phenomena in natural wind, **Ingenisren-International Edition**, 1958, 2, 121–158
[45] CIBSE, CIBSE Guide A: Environmental Design, 2015, IBSN 978-1-906846-54-1

Nomenclature

u	velocity magnitude (m/s)
X, Y, Z	Cartesian co-ordinates (m)
Re	Reynolds number
ρ	air density (kg/m^3)
μ	kinematic viscosity (m^2/s)
Q	volume flow rate (m^3/s)
g	gravitational acceleration (m/s^2)
A	cross-sectional area (m^2)
ΔP	total pressure loss (Pa)
P	pressure (Pa)
P_o	total pressure (Pa)
P_s	static pressure (Pa)
L	length (m)
W	width (m)
H	height (m)
t	time (sec)

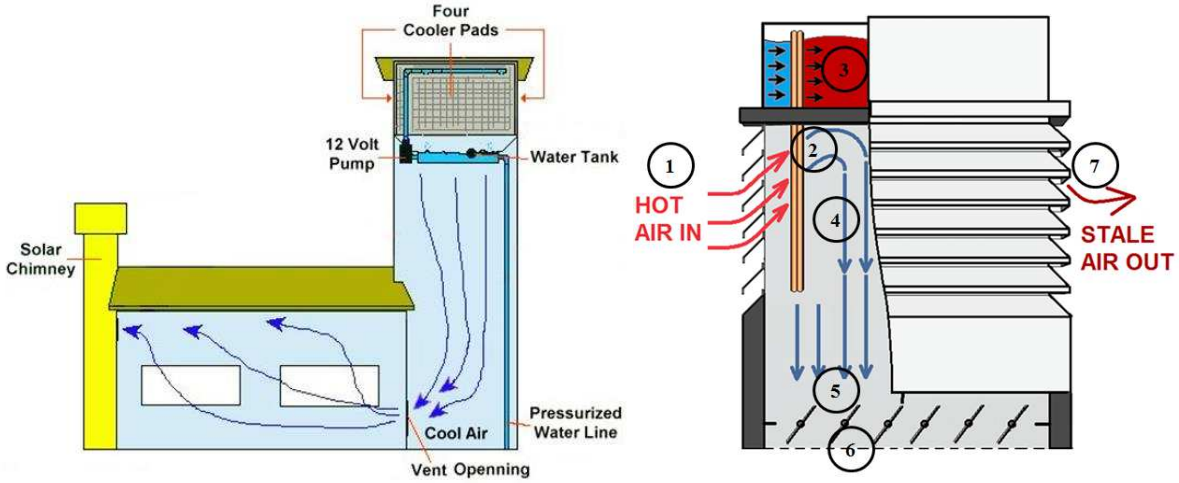

Figure 1 (a) wind tower with evaporative cooling (b) a multi-directional wind tower with VHTDs.

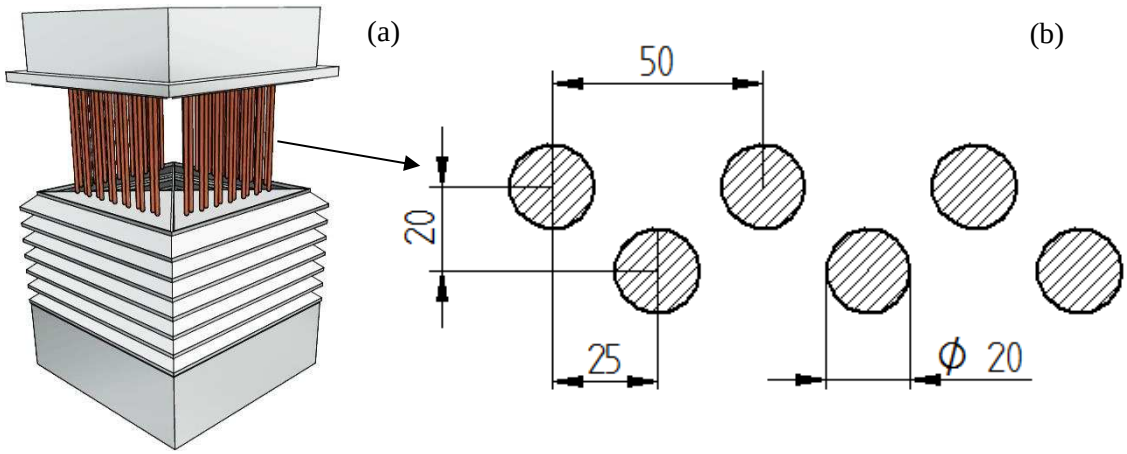

Figure 2 (a) CAD model of the wind tower with VHTD (b) VHTD arrangement and spacing (dimension in mm)**.**

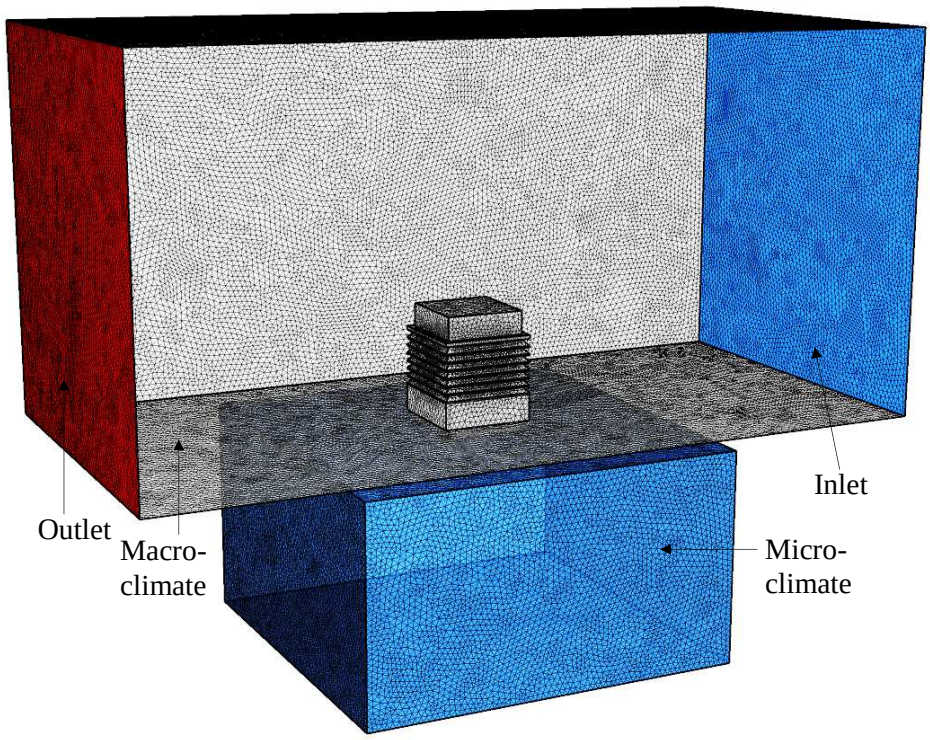

Figure 3 Grid generation on the computational domain.

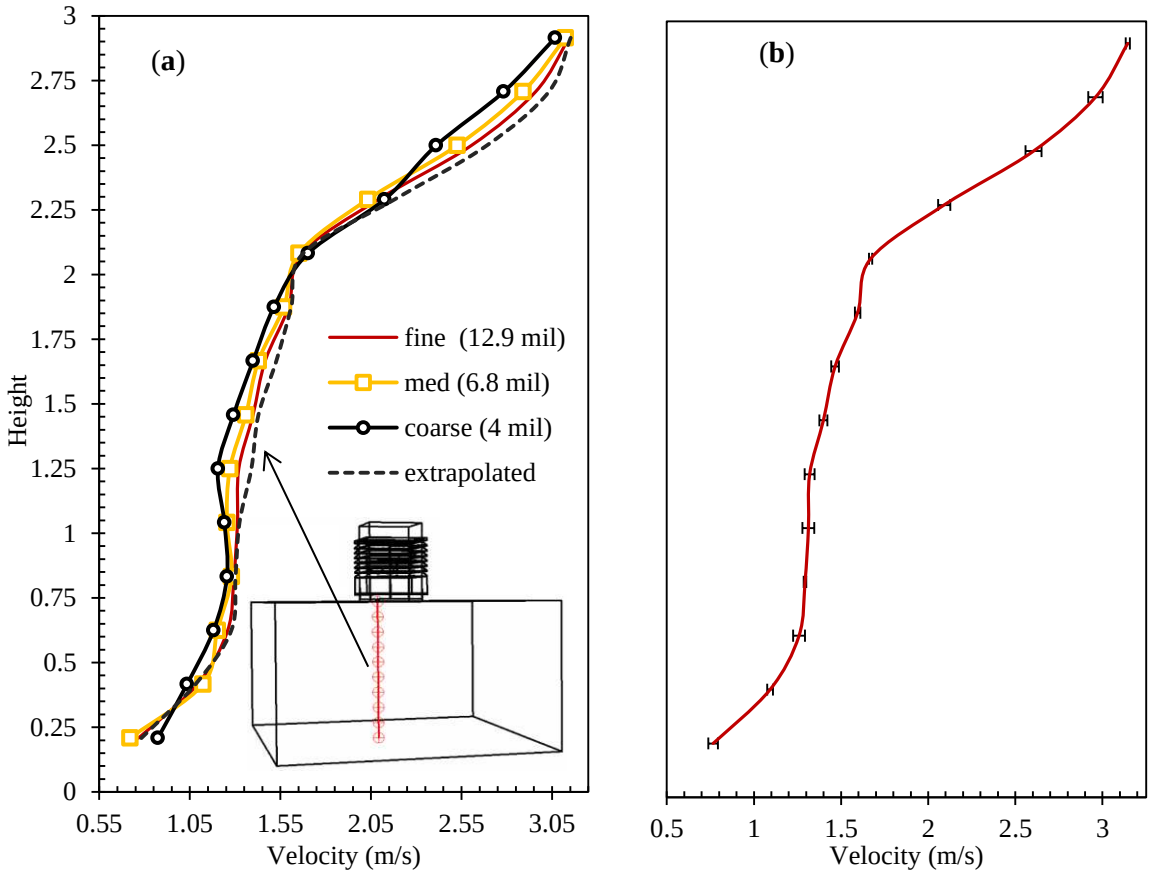

Figure 4 Grid verification using the Grid Convergence (GCI) method. (a) plot of the velocity profiles drawn from a line extending from the supply to the floor; (b) fine grid solution, with discretization error bars computed using the GCI index.

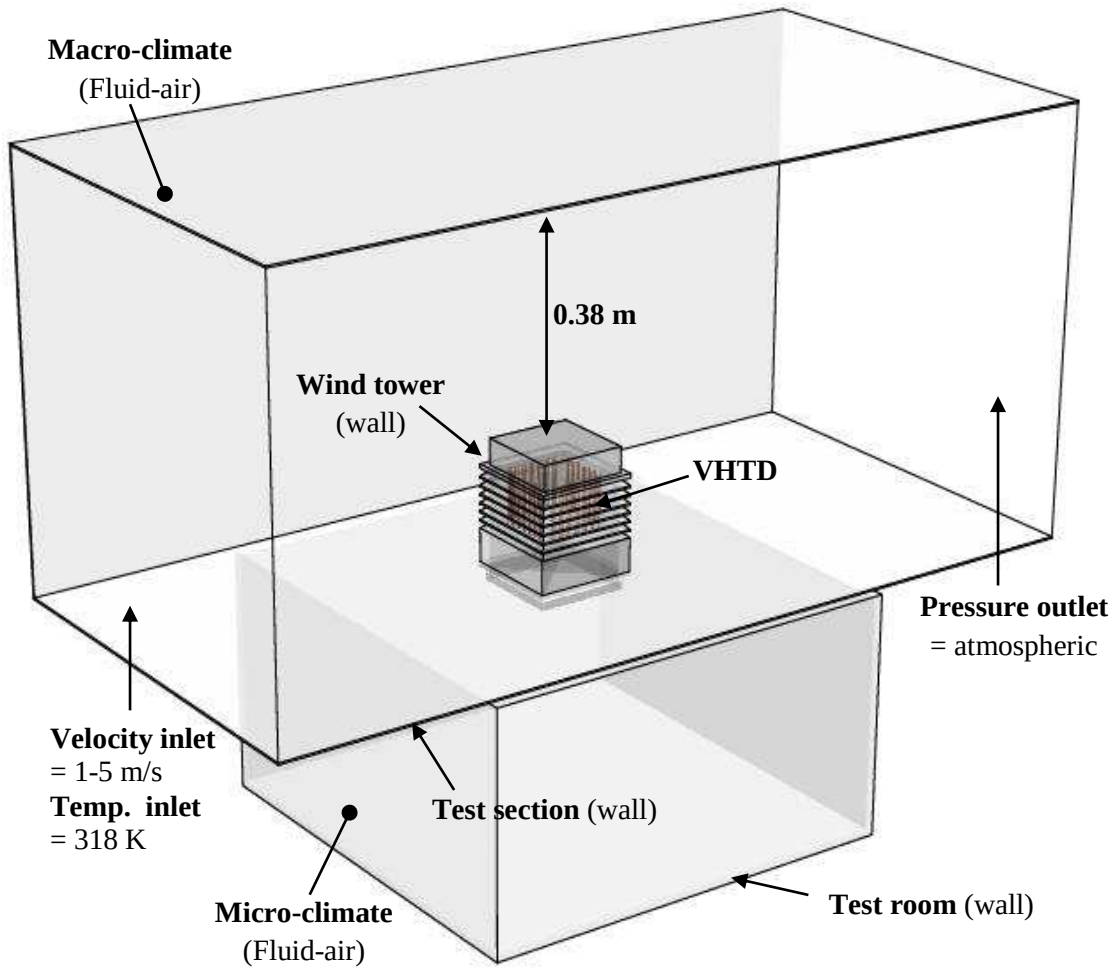

Figure 5 Set boundary conditions for the computational domain's volumes and surfaces.

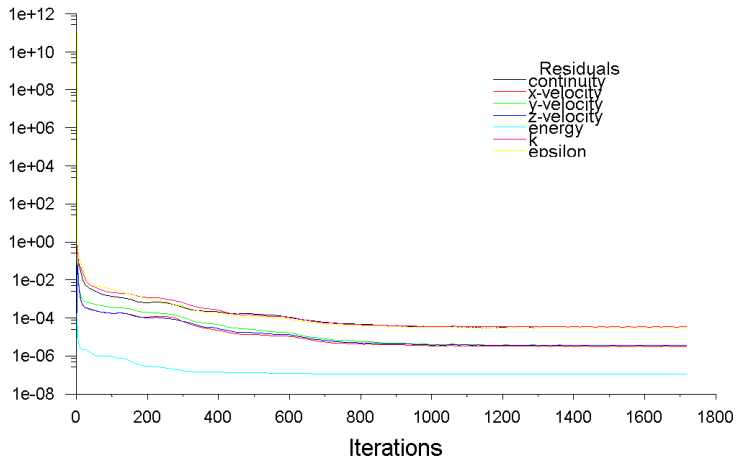

Figure 6 Residuals chart within the Fluent solver.

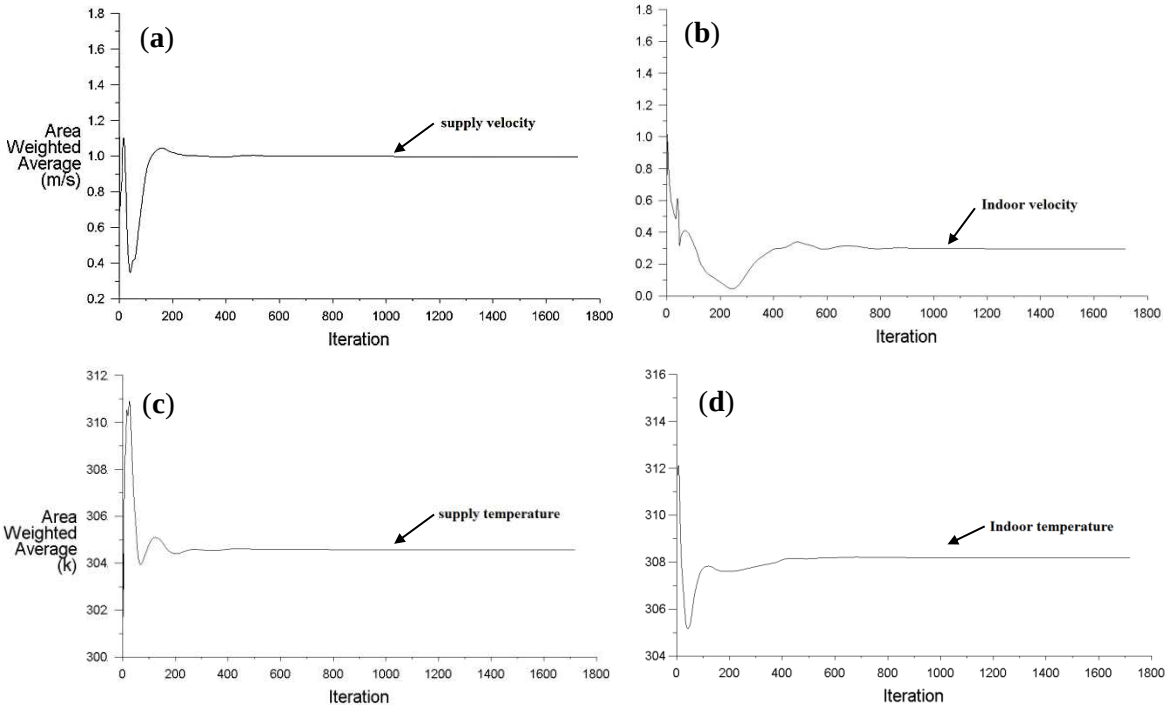

Figure 7 Convergence monitoring of (a) supply velocity (b) indoor velocity (c) supply temperature and (d) indoor temperature.

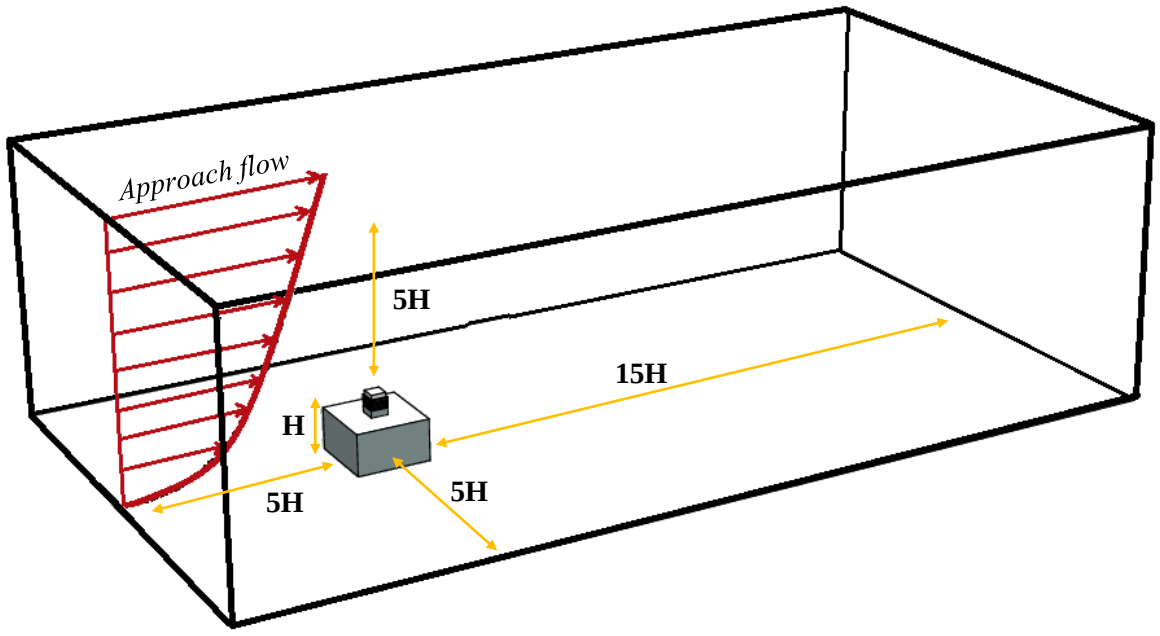

Figure 8 Computational domain for the analysis of the VHTD wind tower in ABL flows.

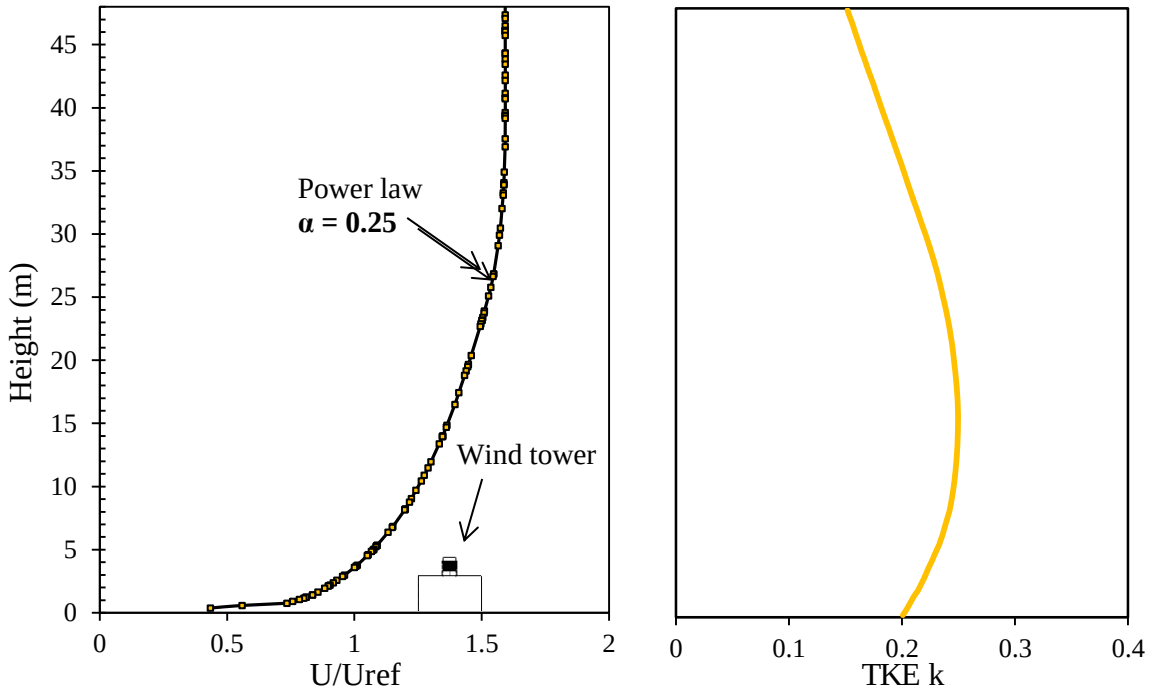

Figure 9 Vertical profiles of (a) mean velocity U and (b) turbulent kinetic energy k in the approaching ABL flow [39].

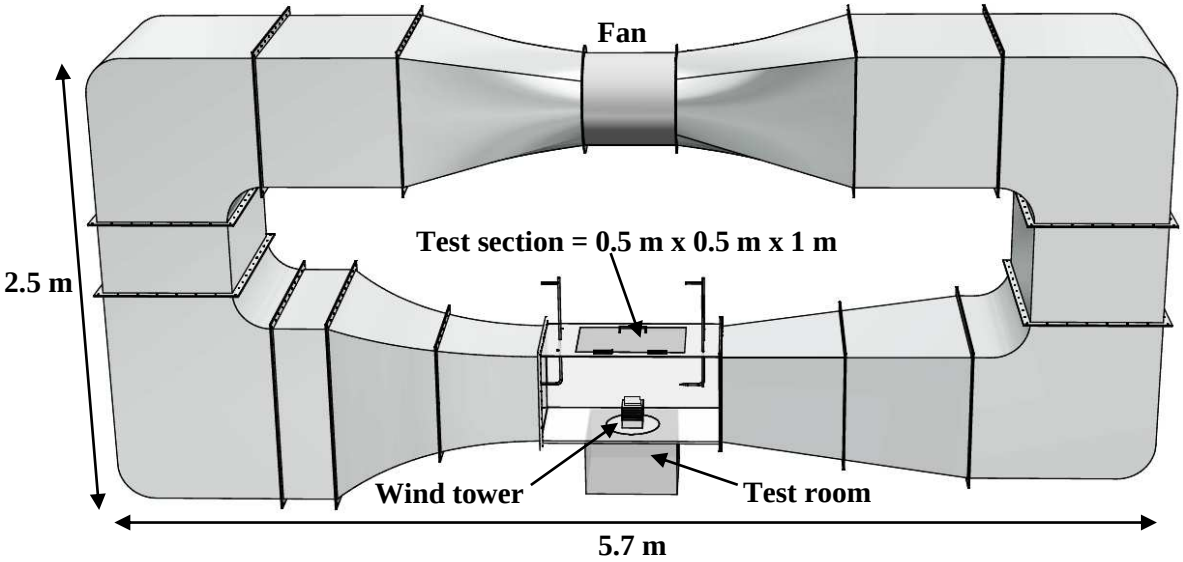

Figure 10 Front view of the closed-loop low-speed wind tunnel [37].

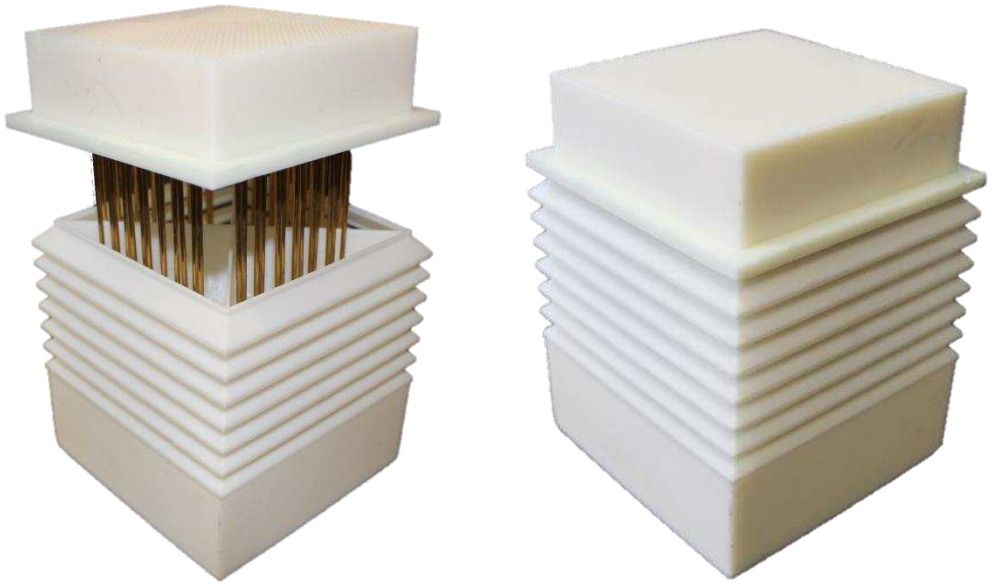

Figure 11 A 1:10 3D-printed model of the VHTD wind tower for the wind tunnel tests.

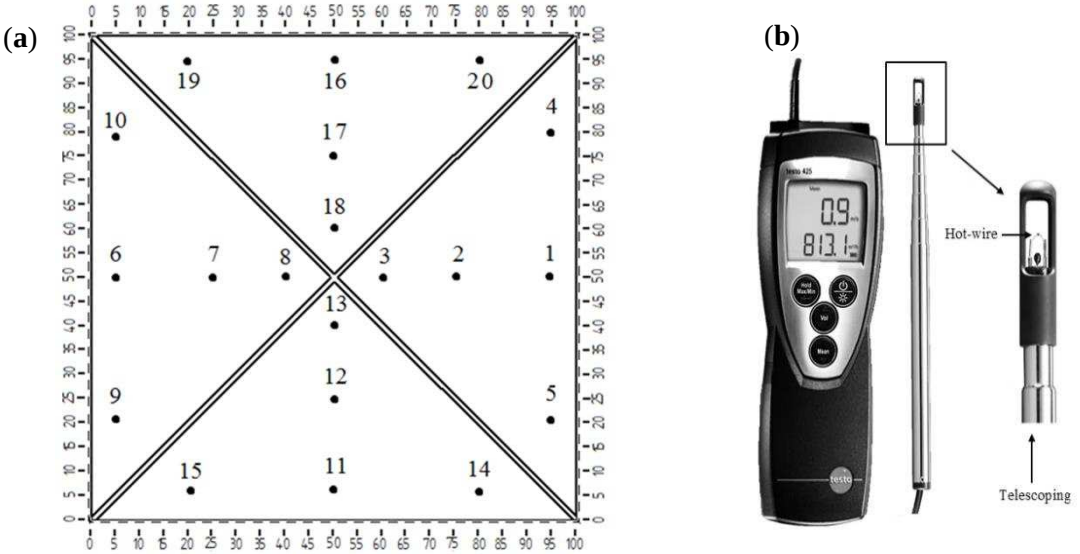

Figure 12 (a) Section view of the wind tower supply channel showing the location of the measurement points (dimensions in mm) (b) hot-wire anemometer.

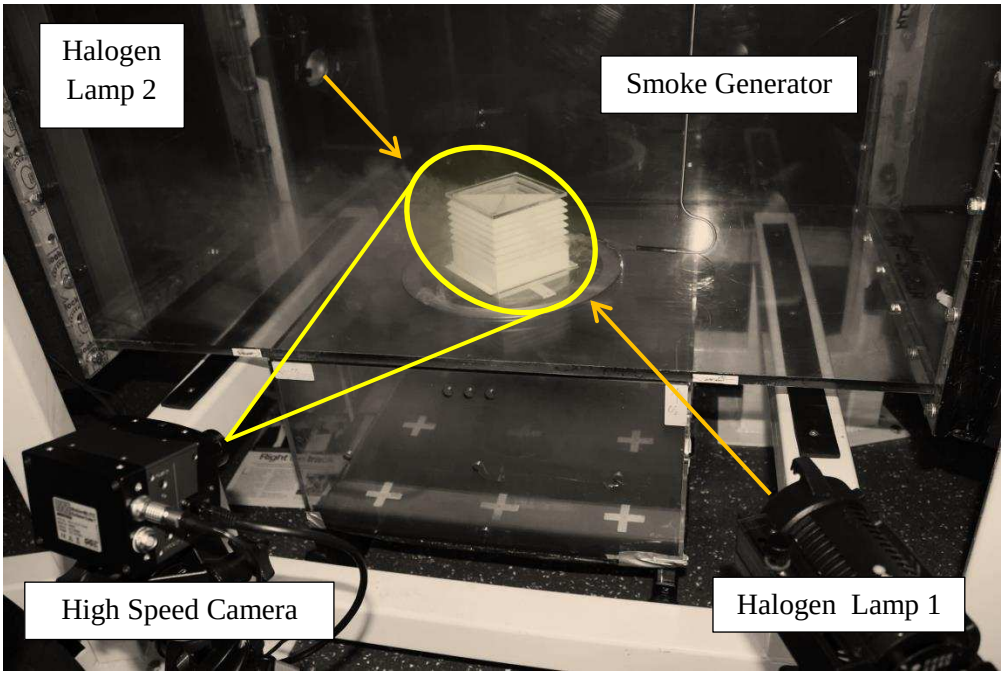

Figure 13 Experimental airflow visualisation test setup.

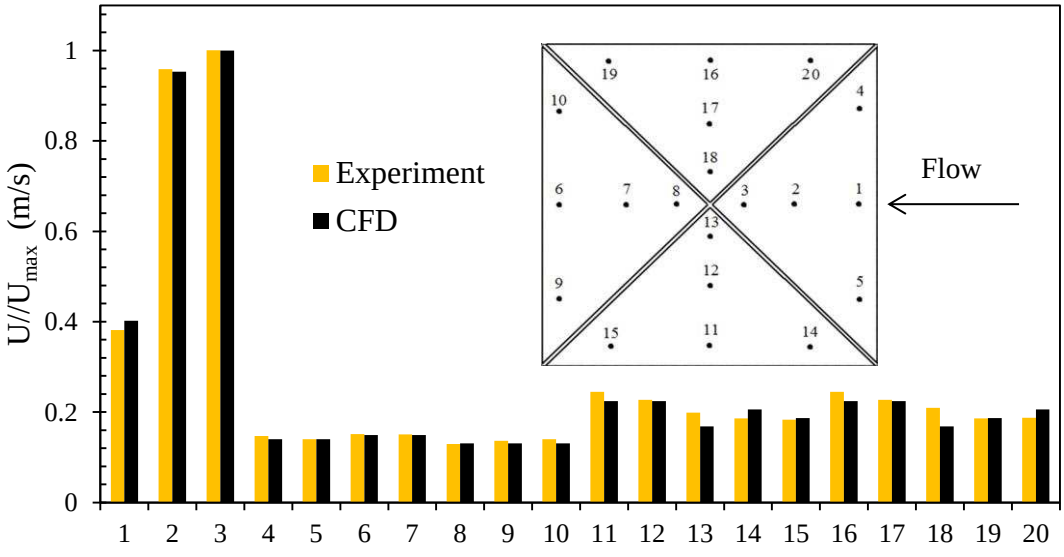

Figure 14 Comparison between predicted and measurement results of the airflow velocity.

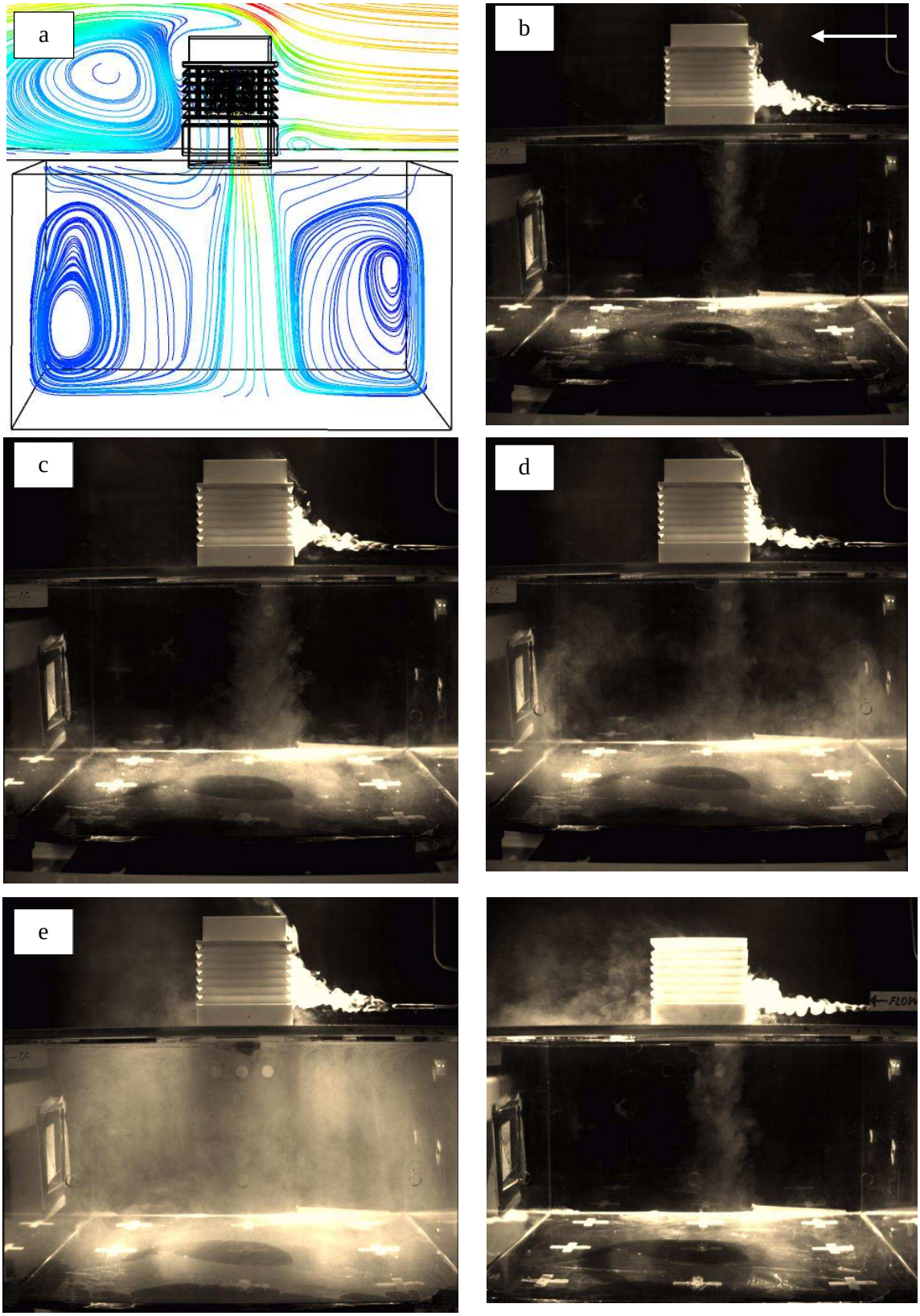

Figure 15 (a) CFD predicted streamlines and video stills of smoke visualisation at (b) 320 millisecond (c) 1000 millisecond (d) 1700 millisecond (e) 3500 millisecond. For comparison, last image shows smoke test of a standard wind tower at 1000 millisecond.

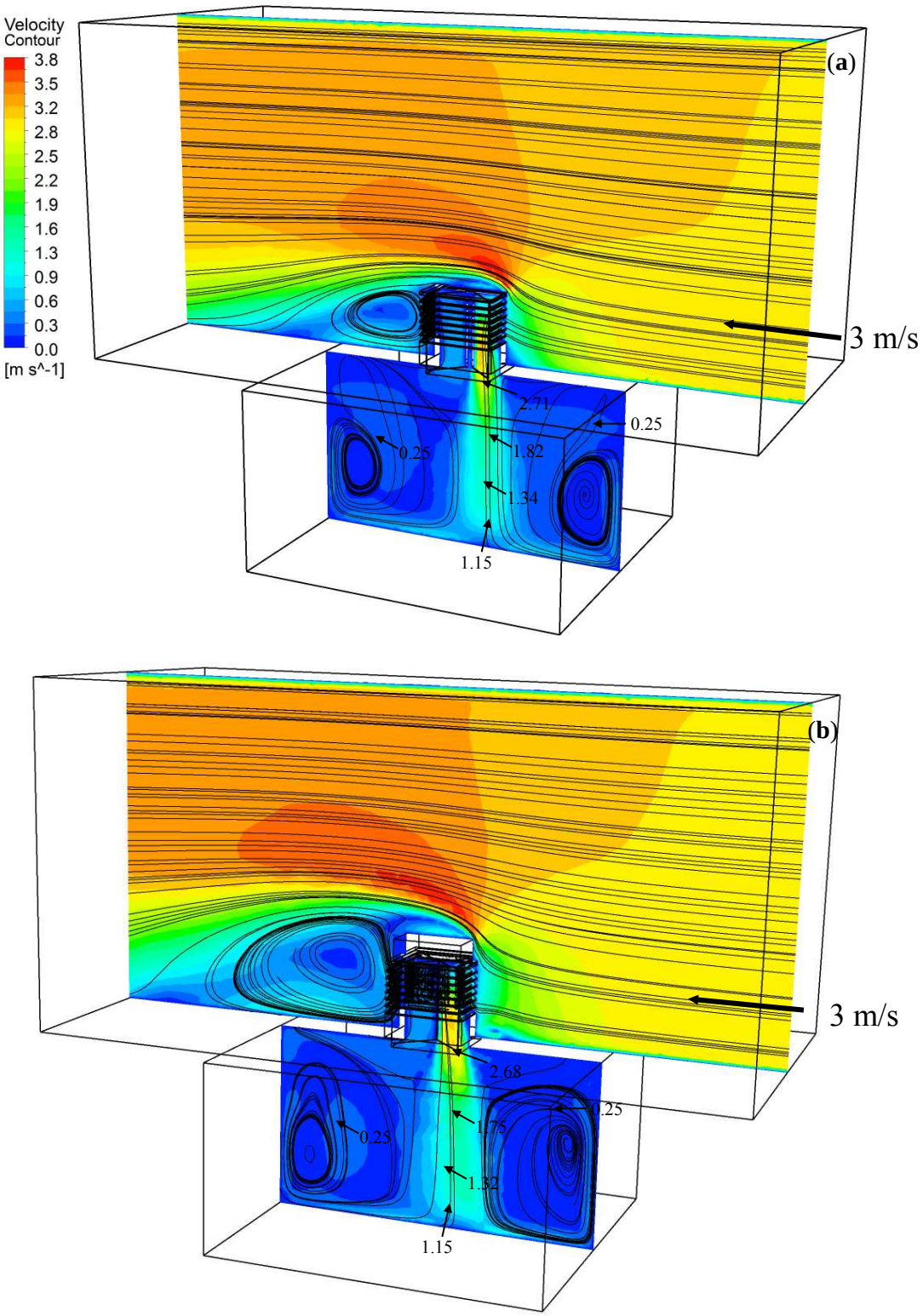

Figure 16 Velocity contour plot of a cross-sectional plane: (**a**) standard wind tower and (**b**) wind tower with vertically-arranged heat transfer devices.

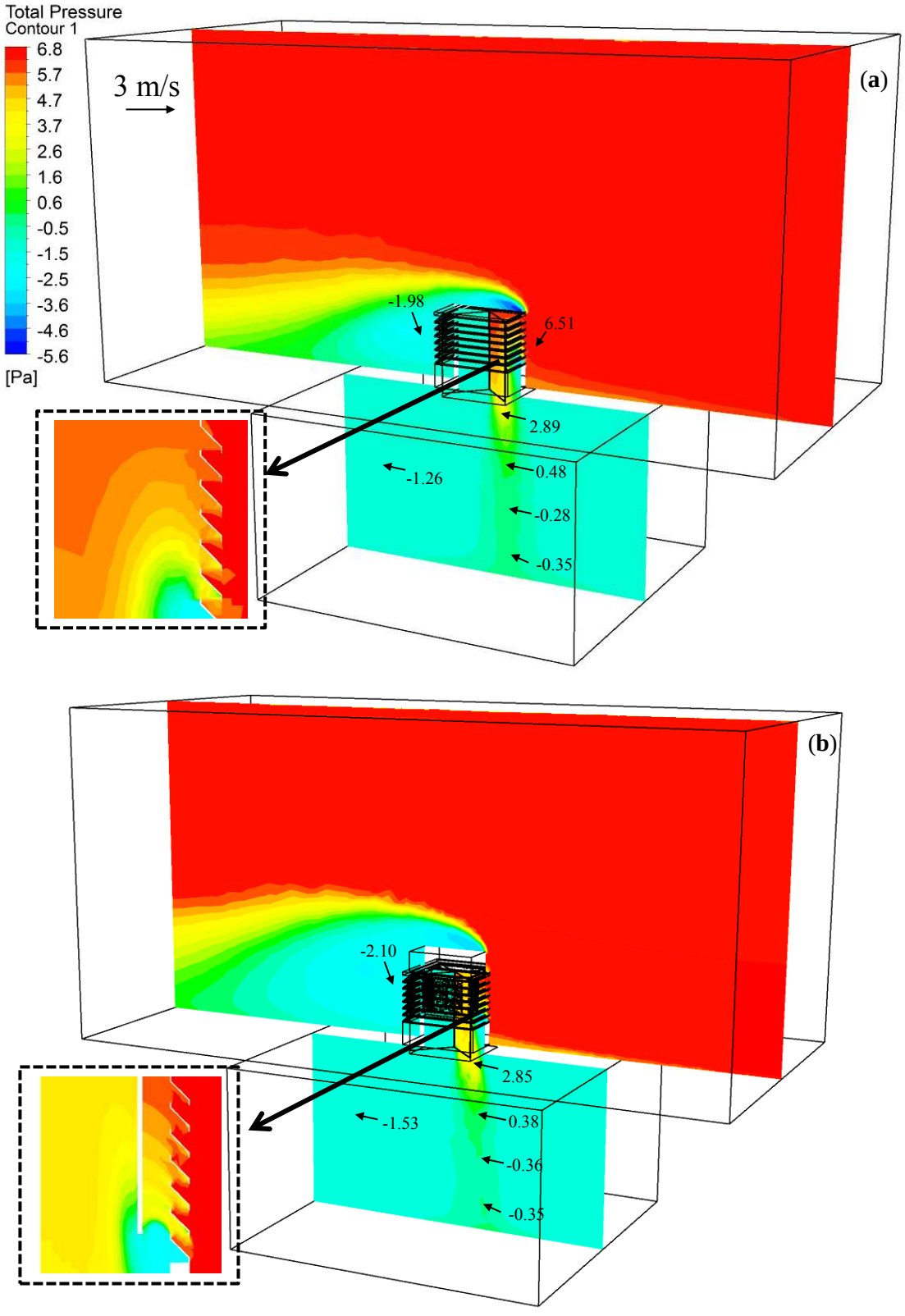

Figure 17 Total pressure contour plot of a cross-sectional plane: (**a**) standard wind tower and (**b**) wind tower with vertically-arranged heat transfer devices.

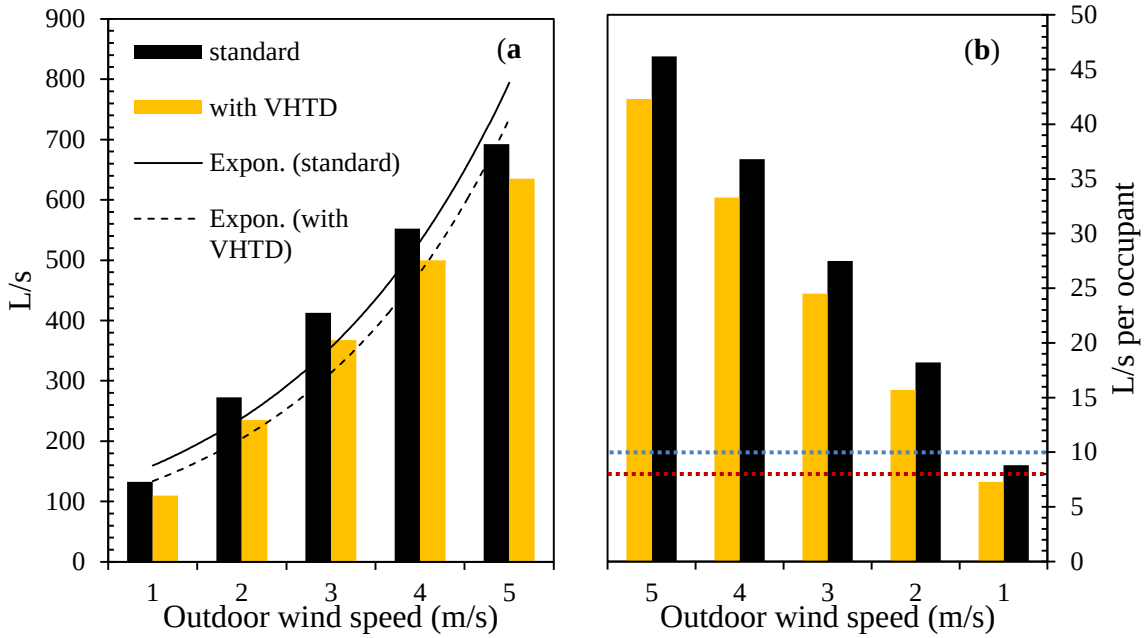

Figure 18 Comparison between the (**a**) airflow supply rates (**b**) L/s per occupant of a standard and VHTD wind tower. Blue dotted lines indicate recommended rate for offices and red dotted lines minimum requirement for classrooms.

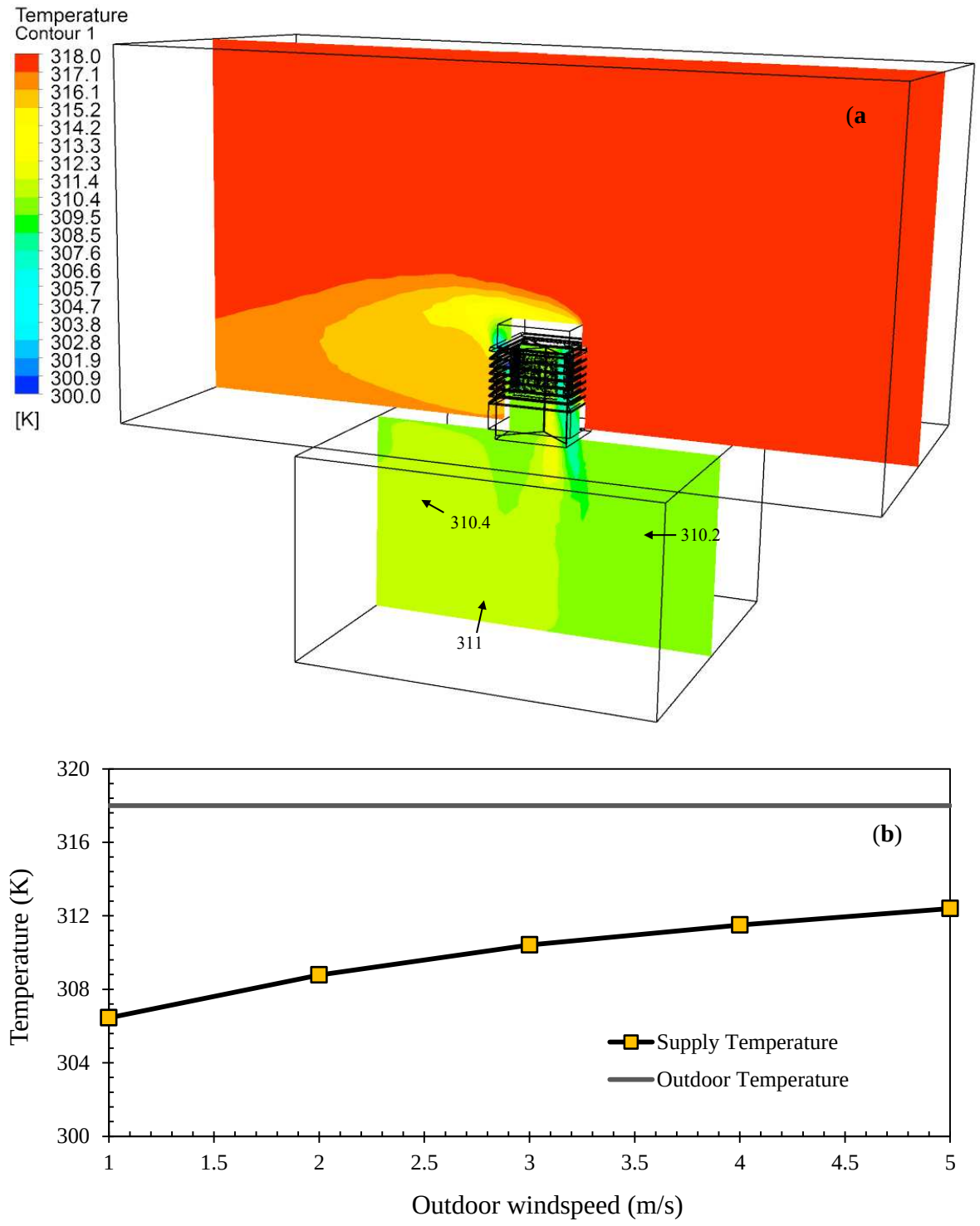

Figure 19 (**a**) Static temperature contour plot of a cross-sectional plane wind tower with vertically-arranged heat transfer devices (**b**) Effect of various outdoor wind speed on average supply temperature.

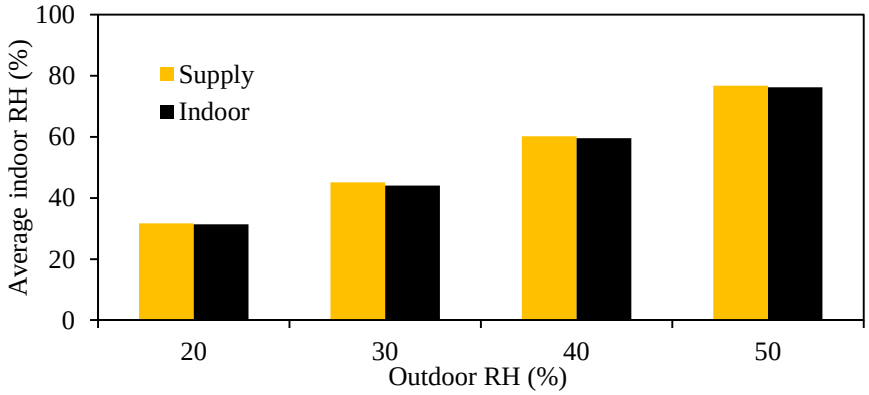

Figure 20 Effect of outdoor relative humidity on average supply temperature, with the outdoor velocity and temperature set at 3m/s and 318K.

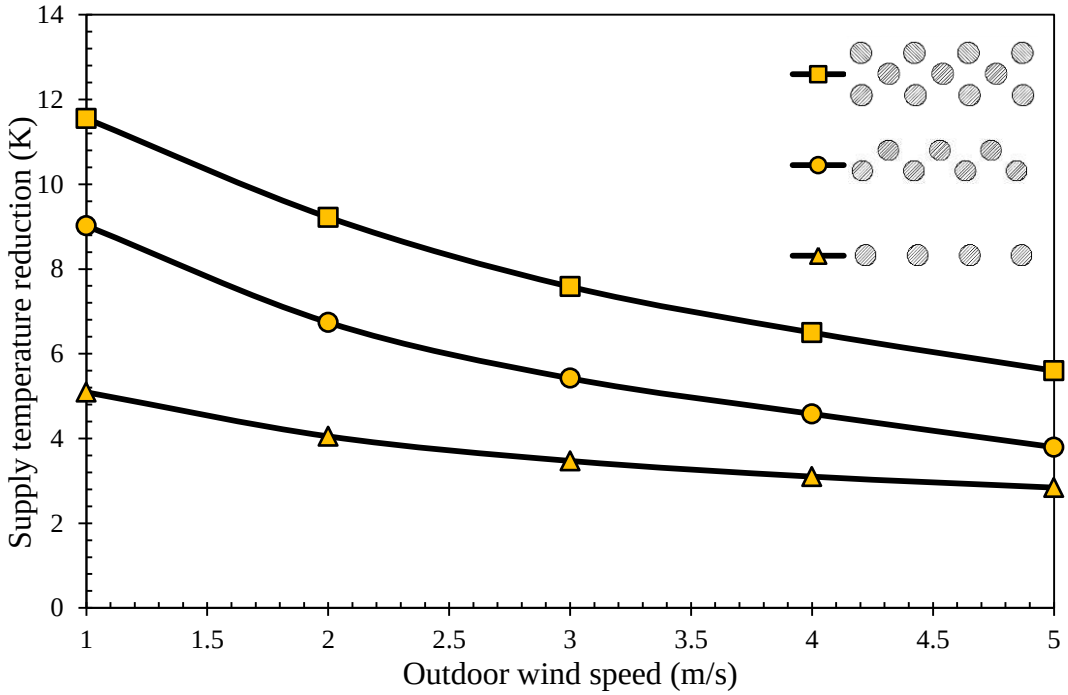

Figure 21 Effect of the variation of HTD rows on supply temperature reduction.

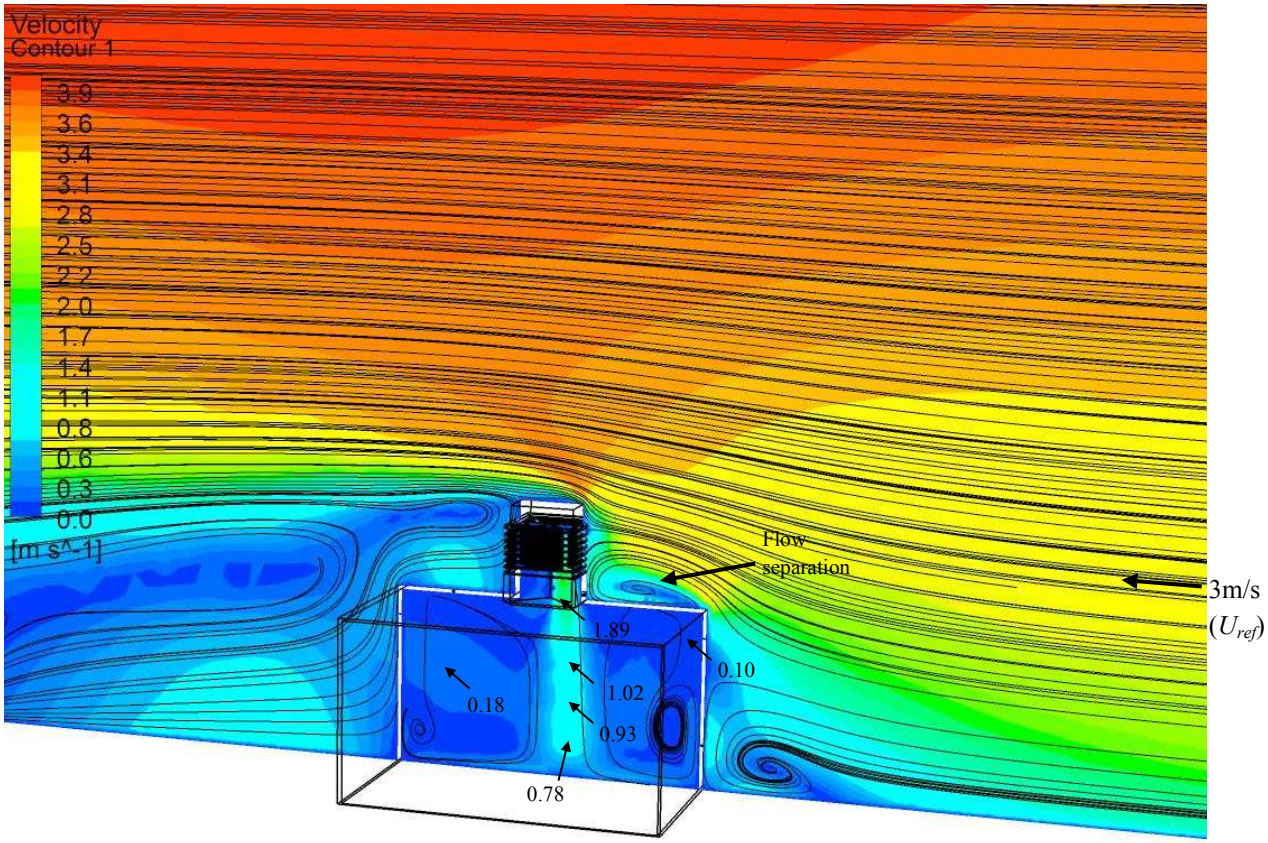

Figure 23 Distribution of the predicted velocity magnitude (m/s) for a wind tower with vertically-arranged heat transfer devices in ABL flows.

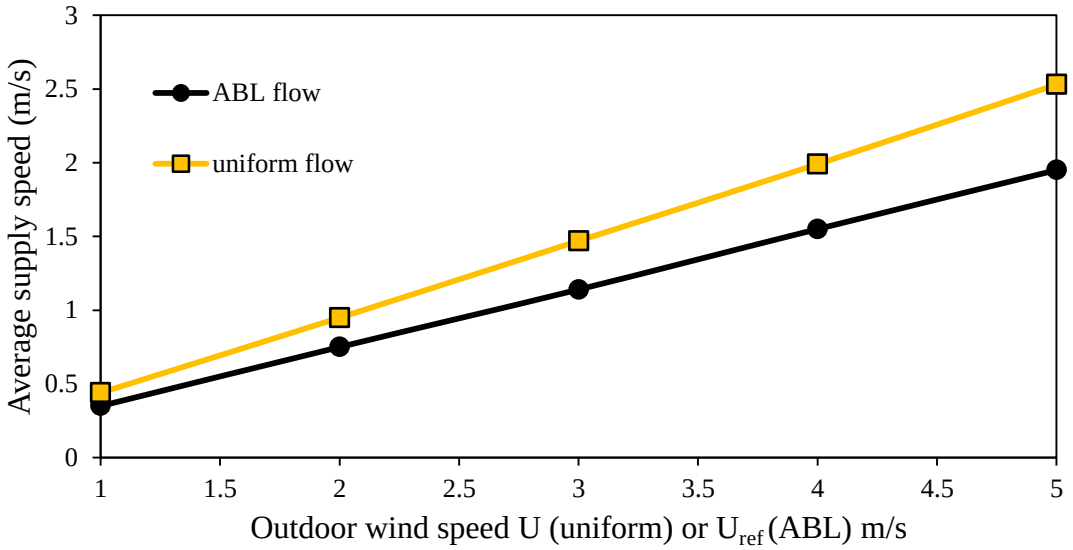

Figure 24 Comparison between the supply speed of the wind tower in uniform and ABL flows ($\alpha = 0.25$) at various outdoor speeds.

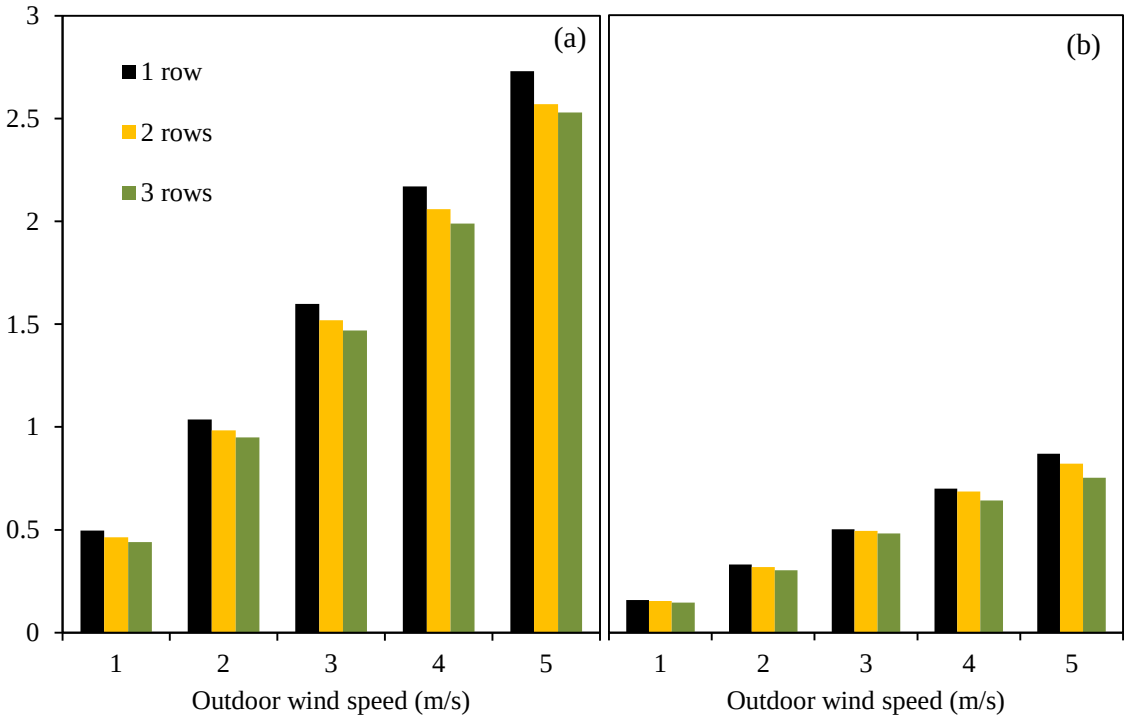

Figure 22 Effect of the variation of HTD rows on (**a**) supply and (**b**) exhaust velocity.

Table 1 Sample calculations of discretisation error using the GCI method.

	Velocity at height = 2.29m	Velocity at height = 1.67m	Velocity at height = 0.62m
$\mathbf{C_1, C_2, C_3}$	12,932,488, 6,847,693, 4,046,918	12,932,488, 6,847,693, 4,046,918	12,932,488, 6,847,693, 4,046,918
$\mathbf{r_{21}}$	1.3742	1.3742	1.3742
$\mathbf{r_{32}}$	1.3007	1.3007	1.3007
$\emptyset_1$	2.0914	1.4657	1.25879
$\emptyset_2$	2.0323	1.4284	1.20171
$\emptyset_3$	2.1254	1.3991	1.18089
p	1.6023	1.4909	4.2045
$\emptyset_{ext}^{21}$	2.1803	1.5272	1.2791
e_a^{21}	2.82%	2.55%	4.53%
$\emptyset_{ext}^{21}$	4.07%	4.03%	1.59%
GCI_{fine}^{21}	**5.31%**	**5.25%**	**2.02%**